Cloud Condensation Nuclei Activity of Internally Mixed Particle Populations at a Remote Marine Free Troposphere Site in the North Atlantic Ocean

Zezhen Cheng[1], Megan Morgenstern[2], Silvia Henning[3], Bo Zhang[4], Gregory C. Roberts[5,6], Matthew Fraund[7], Matthew A. Marcus[8], Nurun Nahar Lata[1], Paulo Fialho[9], Lynn Mazzoleni[2], Birgit Wehner[3], Claudio Mazzoleni[2], Swarup China[1]

[1] Environmental Molecular Sciences Laboratory, Pacific Northwest National Laboratory (PNNL), Richland, WA 99352, USA

[2] Atmospheric Sciences Program, Michigan Technological University, Houghton, Michigan, 49921, USA

[3] Leibniz Institute for Tropospheric Research, Permoserstraße 15, 04318 Leipzig, Germany

[4] National Institute of Aerospace, Hampton, VA 23666, USA

[5] Centre National de Recherches Météorologiques, Université de Toulouse, Météo-France, CNRS, Toulouse, 31400, France

[6] Scripps Institution of Oceanography, University of California San Diego, La Jolla, CA, 92037, USA

[7] Sonoma Technology, Inc., Petaluma, CA 94954, USA

[8] Advanced Light Source, Lawrence Berkeley National Laboratory, Berkeley, CA 94720, USA

[9] Institute of Volcanology and Risk Assessment – IVAR, Rua da Mãe de Deus, 9500-321 Ponta Delgada, Portugal

Correspondence to: Swarup China (swarup.china@pnnl.gov)

Highlights

- Individual particle composition provides a reliable estimation of the hygroscopicity of ambient particles.
- Particle populations consisting of smaller particles are more homogeneous and internally mixed due to higher degrees of atmospheric aging.
- Particles in air masses with high contribution from the marine boundary layer are more active cloud condensation nuclei.

Abstract.

This study reports results from research conducted at the Observatory of Mount Pico (OMP), 2225 m above mean sea level on Pico Island in the Azores archipelago in June and July 2017. We investigated the chemical composition, mixing state, and cloud condensation nuclei (CCN) activities of long-range transported free tropospheric (FT) particles. FLEXible PARTicle Lagrangian particle dispersion model (FLEXPART) simulations reveal that most air masses that arrived at the OMP during the sampling period originated in North America and were highly aged (average plume age >10 days). We probed size-resolved chemical composition, mixing state, and hygroscopicity parameter (κ) of individual particles using computer-controlled scanning electron microscopy with an energy-dispersive X-ray spectrometer (CCSEM-EDX). Based on the estimated individual particle mass from elemental composition, we calculated the mixing state index, χ. During our study, FT particle populations were internally mixed (χ of samples are between 53% and 87%), owing to the long atmospheric aging time. We used data from a miniature Cloud Condensation Nucleus Counter (miniCCNC) to derive the hygroscopicity parameter, κ_{CCNC}. Combining κ_{CCNC} and FLEXPART, we found that air masses recirculated above the North Atlantic Ocean with lower mean altitude had higher κ_{CCNC} due to the higher contribution of sea salt particles. We

used CCSEM-EDX and phase state measurements to predict single-particle κ ($\kappa_{CCSEM\text{-}EDX}$) values, which overlap with the lower range of κ_{CCNC} measured below 0.15% SS. Therefore, CCSEM-EDX measurements can be useful in predicting the lower bound of κ, which can be used in climate models to predict CCN activities, especially in remote locations where online CCN measurements are unavailable.

1. Introduction

Atmospheric aerosol particles can affect climate indirectly by serving as cloud condensation nuclei (CCN), altering cloud lifecycle and albedo (Baustian et al., 2012; Bellouin et al., 2020; Bhattu and Tripathi, 2015; Ervens et al., 2011; Fan et al., 2016; Knopf et al., 2018; Myhre et al., 2013; Seinfeld et al., 2016; Sun and Ariya, 2006). However, our knowledge of aerosol-cloud interactions is still limited, leading to significant uncertainties in predicting the Earth's energy balance (Forster et al., 2021). Part of these uncertainties might be due to the persistent gaps in the fundamental understanding of the ambient CCN number concentration (N_{CCN}), which depends on the particles' hygroscopicity. Petters and Kreidenweis, 2007 proposed a single parameter, the hygroscopicity parameter (κ), based on the κ-Köhler theory to describe particles' hygroscopicity. However, the global distribution of the κ is highly variable due to the complex physicochemical and morphology properties of atmospheric particles (Pringle et al., 2010; Riemer et al., 2019), complicating the prediction of CCN activities in climate models. Typically, atmospheric particles contain both carbonaceous (e.g., black carbon and organic carbon) and inorganic (e.g., sulfate, nitrate, ammonium, sea salts, and dust) species depending on the source (Kolb and Worsnop, 2012; Philip et al., 2014; Pöschl, 2005). Particles also come in a wide range of sizes (from nanometer to micrometer scale) and κ values (from 0 for hydrophobic species to >1 for hydrophilic species) (Ching et al., 2019; Kristensen et al., 2016; Petters and Kreidenweis, 2013, 2007; Pringle et al., 2010; Schulze et al., 2020). Moreover, these different particle species can be internally (distributed within the same particle) or externally mixed (existing as individual particles) in the particle population (China et al., 2015, 2013; Ching et al., 2019; Laskin et al., 2015; Pham et al., 2017; Riemer et al., 2019; Stevens and Dastoor, 2019). This complexity results in highly variable hygroscopicity values and the abilities of

the particles to act as CCN. For example, Li et al., 2021 show that the hygroscopicity of ammonium sulfate (hygroscopic) decreases with the increasing thickness of α-pinene secondary organic aerosol (SOA, less hygroscopic) coating. Moreover, most model simulations assume a homogenous mixing state in the aerosol particle population and use a single κ value, not capturing the variability in individual particles' κ values (Su et al., 2010). Furthermore, the physicochemical properties of particles are continuously modified by several processes during the atmospheric transportation processes (e.g., atmospheric aging, coagulation, condensation, and heterogeneous reactions), complicating our understanding of their roles as CCN (Bond et al., 2013; Laskin et al., 2015; Riemer et al., 2019; Stevens and Dastoor, 2019). Therefore, to reduce uncertainties when predicting atmospheric particles' CCN activities in climate models, it is essential to have a more comprehensive understanding of the influence of chemical composition and mixing state on the particles' κ values.

Typically, κ can be calculated based on in situ CCN counter measurement using the κ-Köhler theory (Petters and Kreidenweis, 2007), which has been widely used for ambient particles (Forestieri et al., 2018; Kawana et al., 2016; Kristensen et al., 2016; Pöhlker et al., 2016) and lab generated particles (Forestieri et al., 2018; Lambe et al., 2011; Petters et al., 2009). However, this method might suffer from limited numbers of supersaturation (SS) ratios and measurements below 0.2% SS due to water depletion and kinetic limitations (Lance et al., 2006; Lathem and Nenes, 2011; Tao et al., 2023; Wang et al., 2019). Another widely used method utilizes aerosol mass spectrometers (AMS) to derive the κ value of particles based on chemical composition (Bhattu et al., 2016; Chang et al., 2010; Fan et al., 2020; Ovadnevaite et al., 2017; Wu et al., 2016). For instance, Ovadnevaite et al., 2017 used AMS to study the influence of liquid-liquid phase separation on the particle's surface tension, which can affect their CCN activation.

Both methods provide an excellent opportunity to reduce uncertainties in CCN prediction related to highly variable κ values, and a combination of both methods can improve our knowledge of the correlation between chemical composition and κ values. Several studies have been conducted at the ground level (Jurányi et al., 2013; Lance et al., 2013; Leck and Svensson, 2015; Vestin et al., 2007; Wang et al., 2010), in the laboratory (Altaf et al., 2018; Fofie et al., 2018; Hatch et al., 2008; R. C. Sullivan et al., 2009), and CCN closure simulation (Bhattu and Tripathi, 2015; Ching et al., 2017; Ren et al., 2018). However, only a limited number of studies have been performed at remote free troposphere (FT) sites (e.g., Schulze et al., 2020) to investigate the relationship between the aerosol chemical composition and mixing state and their CCN roles.

Particles in the FT play an essential role as CCN (Kammermann et al., 2010; Rose et al., 2017; Schulze et al., 2020; Williamson et al., 2019) and can also be transported to the boundary layer via entrainment (De Wekker and Kossmann, 2015; Igel et al., 2017), dry and wet deposition (Igel et al., 2017; Zufall and Davidson, 1998), and dry intrusions (Ilotoviz et al., 2021; Raveh-Rubin, 2017; Raveh-Rubin and Catto, 2019; Tomlin et al., 2021), representing a significant source of CCN in regions with low local emissions such as in the equatorial pacific boundary layer and the arctic (Clarke et al., 2013; Igel et al., 2017). However, it is challenging to perform in-situ CCN measurements at remote FT sites since the deployment of instruments might be difficult and expensive, and the mass concentration of particles is often low (typically ranging from 10^2 to 10^3 particles cm^{-3}) (Allen et al., 2021; Igel et al., 2017; Rose et al., 2017; Schmeissner et al., 2011; Sun et al., 2021). In such cases, offline single-particle microscopy analysis on aerosol particles collected on substrates is a valuable option for low particle loadings (requires in the order of 10^3 particles/substrate). One example of such analysis is using Electron Microscopy coupled

with an Energy Dispersive X-Ray Analysis (EDX) to determine the atomic percentage of elements in individual particles and estimate the average κ values (Ching et al., 2019, 2017). Another example is using scanning transmission X-ray microscopy with near-edge X-ray absorption fine structure spectroscopy (STXM- NEXAFS) to calculate κ values of individual particles using their organic volume fraction (OVF) (Tomlin et al., 2021).

In this study, we present a single-particle analysis of FT particles collected at the Observatory of Mount Pico (OMP) in June and July of 2017. Details for the chemical composition of collected samples, the simulated transport trajectories calculated from the FLEXible PARTicle Lagrangian particle dispersion model (FLEXPART), atmospheric aging time, and CO source of air mass were discussed in Cheng et al., 2022. The present study focuses on the influence of chemical composition and mixing state on the κ values for particles sampled from FT environments based on micro-spectroscopy techniques. We also performed in situ CCN measurements to retrieve κ values. Comparing κ values from offline measurements with those from in situ measurements is used to estimate the offset of offline κ values, improving future applications of this method in climate models.

2. Materials and methods

2.1. Sampling site, online measurements, and sample collection for offline analysis

The site is located at 2225 m above sea level in the summit caldera of the Pico Volcano on Pico Island in the Azores archipelago in the North Atlantic. OMP is an excellent location to investigate the long-range transportation of FT particles above the North Atlantic Ocean during summer due to the negligible influence of local emissions and the marine boundary layer (China et al., 2015; Dzepina et al., 2015;

Honrath et al., 2004; Schum et al., 2018; Val Martin et al., 2008). Details of sampling times and conditions can be found in Cheng et al., 2022 and Table S2. Briefly, FT particle samples were collected during June and July 2017 at OMP using a four-stage cascade impactor (MPS-4G1) on TEM B-film grids (300 mesh, Ted Pella, Inc) with a flow rate of ~7 lpm for multi-modal micro-spectroscopy analysis. Particles collected on the third and fourth stages have 50% cutoff diameters of 150 and 50 nm, respectively. Due to the limited transportation events and difficulty of accessing the OMP, coordinating offline sample collection with pollution transportation linked to specific sources is challenging. Thus, in this study, we only collected four Stage 3 samples (S3-1 to S3-4) and four Stage 4 samples (S4-1 to S4-4). From July 5th to 22nd, at OMP, a Scanning Mobility Particle Sizer (SMPS, TROPOS home-built (Wiedensohler et al., 2012)) and a miniature Cloud Condensation Nucleus Counter (miniCCNC) (Roberts and Nenes, 2005; Wex et al., 2016) were also operated to monitor the particle size distribution, total particle concentration, and CCN concentration. The miniCCNC was operated in flow scanning mode, and CCN number concentrations were measured at 10 SS ratios (0.10%, 0.12%, 0.15%, 0.18%, 0.21%, 0.26%, 0.32%, 0.38%, 0.46%, and 0.55%) every 13 mins. The uncertainties in SS ratios is roughly 10% of SS ratios due to a combination of flow, pressure, and temperature control. The miniCCNC was calibrated at each SS ratio, following the procedure in Rose et al., 2008. The SS ratio was controlled by simultaneously changing the flow rate (from 0.09 to 0.22 LPM) through the instrument column and the temperature gradient, allowing a fast response. We also fixed the column's bottom temperature and minimized the temperature difference between that and the optical cavity to avoid evaporating the activated droplets, which caused the CCN instrument to undercount the CCN concentration. Due to the low particle concentration, we minimized the sheath-to-aerosol (SAR) ratio to maximize counting statistics (Lathem and Nenes, 2011). Moreover, since the CCN concentrations during this campaign are well below the

concentrations needed for kinetic limitations (Lathem and Nenes, 2011), particles should be able to activate at their critical supersaturation ratio. Previous studies have shown that the miniCCNC can provide valid data below 0.2% SS (Hammer et al., 2014; Saliba et al., 2021; Ryan C. Sullivan et al., 2009; Sullivan et al., 2010; Wex et al., 2016). Experimental details of the CCN and size distribution measurements were reported elsewhere (Siebert et al., 2021).

2.2. Backward trajectory analysis using FLEXPART simulation

The retroplume analysis using FLEXPART (Owen and Honrath, 2009; Seibert and Frank, 2004; Stohl et al., 2005) allow the establishment of the origin and transport trajectories for the air mass arriving at OMP during offline sample collection and CCN measurements. FLEXPART simulation details for the period under study can be found in Cheng et al., 2022. Briefly, the transport trajectories were obtained by integrating the FLEXPART simulated matrices of air mass residence time over time and altitudes, which revealed general transport pathways for analyzed particle samples. Since particles and many of their precursors are usually co-emitted with CO from anthropogenic and wildfire sources, the sources and ages of particle samples were also estimated based on the FLEXPART CO tracer calculation. We estimated the impact of such sources from different continents on our analyzed particle samples by coupling CO emission inventories with FLEXPART simulated residence time. Since aging is critical to particle properties, we also calculated the averaging FLEXPART CO ages (transport time from sources to OMP) for each particle sample approximately as a particle aging indicator (Zhang et al., 2017, 2014).

2.3. Microscopy and spectroscopy analysis of individual particles

The samples collected at OMP were analyzed with computer-controlled scanning electron microscopy with an energy-dispersive X-ray spectrometer (CCSEM-EDX) to probe their physicochemical properties (Laskin et al., 2006, 2005). Details are provided by Cheng et al., 2022. Briefly, an environmental SEM (ESEM) equipped with an FEI Quanta digital field emission gun, operated at 20 kV, 480 pA current, was utilized to analyze samples at 293 K and under vacuum conditions (~2×10^{-6} Torr), causing the evaporation of volatile compounds. The individual particles' shape, morphology, and size (projected area equivalent diameter) were retrieved from the ESEM images. The CCSEM was equipped with an EDX spectrometer (EDAX, Inc.), and EDX spectra from individual particles were used to determine the relative atomic percentage of 15 elements (C, N, O, Na, Mg, Al, Si, P, S, Cl, K, Ca, Mn, Fe, and Zn). The relative atomic percentage of all elements was post-corrected as described by Cheng et al., 2022 since lighter elements C, N, and O are considered semi-quantitatively, and there might be considering contributions of C and O from the carbon B-film substrate. Variation of individual particles' aspect ratio (particle width to height ratio) is responsible for uncertainty in the post-correction method. These uncertainties are propagated in all relevant calculations in this study. The validation of the post-correction method is presented in Section S1 in the SI. All samples contain high C, N, and O atomic percentages and low soot fractions, suggesting organic-rich particles. Based on the atomic percentage, each particle was classified as organic (OC), carbonaceous with nitrogen (CNO), carbonaceous with sulfate (CNO with S), sea salt (Na-rich), sea salt with sulfate (Na-rich with S), dust (Al, Si, Ca, and Fe rich), dust with sulfate (Al, Si, Ca, and Fe rich with S), and others (Cheng et al., 2022).

2.4. Mixing state parameters

The particle mixing state defines the different components distributed in the aerosol population (either externally mixed or internally mixed) (Riemer et al., 2019) and the aerosol optical properties (Jacobson, 2001; Lack and Cappa, 2010; Saleh et al., 2015), cloud condensation nuclei activities (Ching et al., 2017; Sánchez Gácita et al., 2017), and wet removal (Koch et al., 2009; Stier et al., 2006) all depend on the mixing state. The mixing state of particle population is calculated from the species mass fractions in a particle and the population (Riemer and West, 2013). The method used to parameterize the mixing state of aerosol samples has been described in detail by Riemer and West, 2013. Briefly, for a given species *a* (*a*=1, 2, …, *A*, with *A* the total number of species) in the ith particle (*i*=1, 2, …, *N*, with *N* the total number of particles analyzed), the mass of species *a* is denoted by μ_i^a. From this basic description of the particles' composition, the total mass of each particle (μ_i), the total mass of element *a* in the sample (μ^a), and the total mass of the sample (μ) are determined:

$$\sum_{a=1}^{A} \mu_i^a = \mu_i \,, \sum_{i=1}^{N} \mu_i^a = \mu^a, \sum_{a=1}^{A} \sum_{i=1}^{N} \mu_i^a = \mu \qquad (1)$$

Hence, the mass fraction of species *a* in particle *i* (p_i^a), the mass fraction of particle *i* in the sample (p_i), and the mass fraction of species *a* in the sample are defined as:

$$p_i^a = \frac{\mu_i^a}{\mu_i}, p_i = \frac{\mu_i}{\mu}, p^a = \frac{\mu^a}{\mu} \qquad (2)$$

Therefore, the Shannon entropy for the species distribution within the particle *i* (H_i), the average per particle (H_α), and the species distribution within a sample (H_γ) are calculated from the mass fractions (equation (2)):

$$H_i = \sum_{a=1}^{A} -p_i^a \, ln \, p_i^a, \; H_\alpha = \sum_{i=1}^{N} p_i H_i \,, H_\gamma = \sum_{a=1}^{A} -p^a \, ln \, p^a \qquad (3)$$

The Shannon entropy quantifies the uniformity of the mass fractions in a given population, which increases when the mass fraction is more uniform across the population. H_i, H_α and H_γ are converted to the particle diversity of particle i (D_i), average particle species diversity (D_α), and the bulk population diversity:

$$D_i = e^{H_i},\ D_\alpha = \mathrm{e}^{H_\alpha},\ D_\gamma = \mathrm{e}^{H_\gamma} \tag{4}$$

These diversity values represent the effective number of species within a given population.

Finally, we calculated the mixing state index (χ) from the average particle species diversity (D_α) and the bulk population diversity (D_γ):

$$\chi = \frac{D_\alpha - 1}{D_\gamma - 1} \tag{5}$$

The χ value indicates a fully externally mixed population (χ = 0% and D_α=1) to a fully internally mixed population (χ = 100% and D_α= D_γ) (Riemer and West, 2013).

In this study, we retrieved χ from post-corrected CCSEM-EDX relative atomic percentage data. Therefore, to calculate the μ_i, we retrieved the absolute mass of individual particles. To achieve this goal, we applied a similar method introduced by O'Brien et al., 2015 and Bondy et al., 2018 but with some modifications since these studies did not include C, N, and O from CCSEM-EDX data in the mixing state calculation. Briefly, we assume that each particle is a mixture of the five species commonly observed in the FT particles at the OMP site: carbonaceous, sulfate, sea salt, dust, and anything else (others) (Cheng et al., 2022; China et al., 2017; Dzepina et al., 2015; Lata et al., 2021; Schum et al., 2018). It should be

noticed that this assumption differs from the particle classification introduced in Section 2.3, and assuming only five species in each particle might underestimate the individual particle diversities. Thus, adding more species and precisely assigning elements in each species could improve the accuracy of this method, which might be a task for future studies.

The density and the assumed molecular formula of each species are listed in Table S1. The density of each particle *i* (ρ_i) is calculated as:

$$\rho_i = \sum_{a=1}^{5} \frac{p_i^a}{\sum_{a=1}^{5} \frac{p_i^a}{\rho_a}} \tag{6}$$

Where p_i^a is the mass fraction of ath specie in particle *i* (total 5 species) retrieved from CCSEM-EDX data, equal to the sum of each element's mass fraction, ρ_a is the density of that species (see Table S1). Since Cheng et al., 2022 have shown that the majority of our particles are in a liquid state with the shape of flat spherical caps upon impaction on the substrate, the volume of each particle (V_i) can be calculated as:

$$V_i = \frac{1}{6}\pi \left(\frac{L_{\text{proj}}}{\overline{\text{AR}}}\right) \left[\frac{3}{4} {L_{\text{proj}}}^2 + \left(\frac{L_{\text{proj}}}{\overline{\text{AR}}}\right)^2\right] \tag{7}$$

Where L_{proj} is the longest projected length of each particle retrieved from SEM images and $\overline{\text{AR}}$ is the average aspect ratio (particle width to height ratio) of the sample retrieved from ESEM tilted images (Cheng et al., 2022, 2021). We note that the aspect ratio of individual particles might deviate from the $\overline{\text{AR}}$, leading to either an overestimate or an underestimate of the volume of individual particles. These potential biases have been included while estimating the relevant uncertainty calculation. Moreover, equation 1 needs to be modified to represent different particle shapes. Therefore, the μ_i is calculated as:

$$\mu_{\mathrm{i}} = \rho_{\mathrm{i}} \times V_{\mathrm{i}} \quad (8)$$

2.5. κ value from miniCCNC measurements

We derived the hygroscopicity parameter (κ) from the equilibrium saturation ratio of water vapor and particle diameter based on κ-Köhler theory (Petters and Kreidenweis, 2007), assuming the particles population are homogeously internally mixed. For the κ-Köhler theory, the Raoult term in the Köhler equation is parameterized by a single parameter, the hygroscopicity parameter κ, defined as:

$$\kappa = \frac{4\left(\frac{4\sigma M_W}{RT\rho_W}\right)^3}{27\, D_{act,d}^3 * ln^2\, SS} \quad (9)$$

where *SS* is the SS ratio (%), M_w is the molar mass of water (18 g/mol), ρ_w is the density of water (1 g/mL), σ is the surface tension of the water/air interface (0.072 J m^{-2}), *R* is the universal gas constant (8.314 J $(K\ mol)^{-1}$), and *T* is the absolute temperature (K).

The equation includes the diameter where a particle is barely large enough to be activated at a given SS and the activation dry diameter ($D_{act,d}$). In general, κ quantifies the affinity of a material for water. For atmospheric particles, the range of κ values spans roughly from 0 (insoluble particles, e.g., soot) to 1.4 (very hygroscopic, e.g., sodium chloride), as shown in Petters and Kreidenweis (2007). Under the assumption of an internally mixed particle population, κ can be calculated by deriving $D_{act,d}$. For that, the measured CCN number concentrations (N_{CCN}) and particle number size distribution (PNSD) are used so that the PNSD is integrated until the resulting particle number concentration, N, is equal to N_{CCN}. The particle diameter at this point is $D_{act,d}$.

2.6. Estimation of κ value from CCSEM-EDX measurements

Based on the Zdanovskii–Stokes–Robinson assumption (Petters and Kreidenweis, 2007), the κ value of internally mixed particles (κ_i) can be estimated by a volume-weighted addition of the κ values of the pure specie:

$$\kappa_i = \sum_{a=1}^{5} \varepsilon_{i,a} \kappa_{i,a} \tag{10}$$

Where ε_a and κ_a are the ath species' volume fraction and hygroscopicity parameters, respectively. To estimate the κ values for individual particles, we assume each particle is a homogeneous mixture of the five species discussed in Section 2.4, and their κ values are listed in Table S1. This assumption is supported by SEM and TEM images of particles discussed in Cheng et al., 2022, and the mixing state index of each sample (see Section 3.3). ε_a is calculated from the parameters used in the mixing state index calculation in eq. 1, 2, and 6 to 8:

$$\varepsilon_a = \frac{V_a}{V_i} = \frac{\mu_i^a}{\rho_a} \frac{\rho_i}{\mu_i} = p_i^a \frac{\rho_i}{\rho_a} \tag{11}$$

Then the κ value for the sample is calculated as the mass-weight average of κ values of individual particles in that sample:

$$\bar{\kappa} = \sum_{i=1}^{i} p_i \times \kappa_i \tag{12}$$

This method estimate the SS ratio independed κ value based on the aerosol composition, which can be used directly in the climate models.

3. Results and Discussions

3.1. Airmass transport patterns based on FLEXPART simulation

In an earlier study (Cheng et al., 2022), we discussed in detail the 20 days back trajectory FLEXPART simulation results, including air masses transport and vertical distribution, CO source contribution, and average atmospheric aging time, for the same particle samples analyzed in this study. The same information for air masses that arrived during online miniCCNC measurements (July 5th to July 22nd, 2017) is shown in Figures S1-S3. Air masses were classified into two cases based on their transport pattern, and representative FLEXPART simulations are shown in Figure 1. Case 1 represents air masses that was transported across North America with a relatively higher average height (Figure 1(a)), and Case 2 represents air masses that recirculated over the North Atlantic Ocean for more than ~10 days with a relatively lower mean height (Figure 1(b)). Case 1 represents July 5th to July 10th and July 19th to July 22nd since air masses were mainly transported across North America (up to ~5 days before reaching OMP) (Figures S1 (a-f and o-r)). The air masses for July 5th to 10th and July 19th to July 20th were transported relatively higher in the FT (average height was ~ 8 km) across North America and stayed at approximately the same altitude until they reached OMP ~5-10 days later (Figure S2 (a-f and o-p)). The average height of air masses for July 20th and July 21st was lower (~5-6 km) when transported over North America (Figure S2 (q and r)). Based on the FLEXPART CO tracer analysis, from July 5th to July 7th and July 19th, air masses were mainly influenced by anthropogenic sources in North America (~47-80% CO contribution). From July 8th to July 10th and July 20th to July 22nd, North America's major CO contribution sources were wildfires (~26-90%) (Figure S3). Case 2 includes July 11th to July 18^{th,} where air masses recirculated over the North Atlantic Ocean for more than ~10 days and received air masses from North America and Africa (Figure S1 (g-n)). These air masses traveled relatively higher in the FT (average height was ~8 km) at ~20 days upwind and then continuously decreased in average height to the lower free troposphere across the Northern Atlantic Ocean until reaching OMP (Figure S2 (g-n)). This path

allowed significant contributions from sea sprays through convection and frontal uplift (North et al., 2014). Besides the contribution from sea spray, CO tracer analysis shows that CO contributions for Case 2 air masses were also influenced by North America anthropogenic emissions (~13.1-85.4 %) and Africa (~0.0-78.9 %). CO tracer analysis also shows that the average CO aging time of all air masses that arrived at OMP during CCN measurements was 14.2±2.3 days (ranging from 9.5 to 18.0 days), indicating they are highly aged.

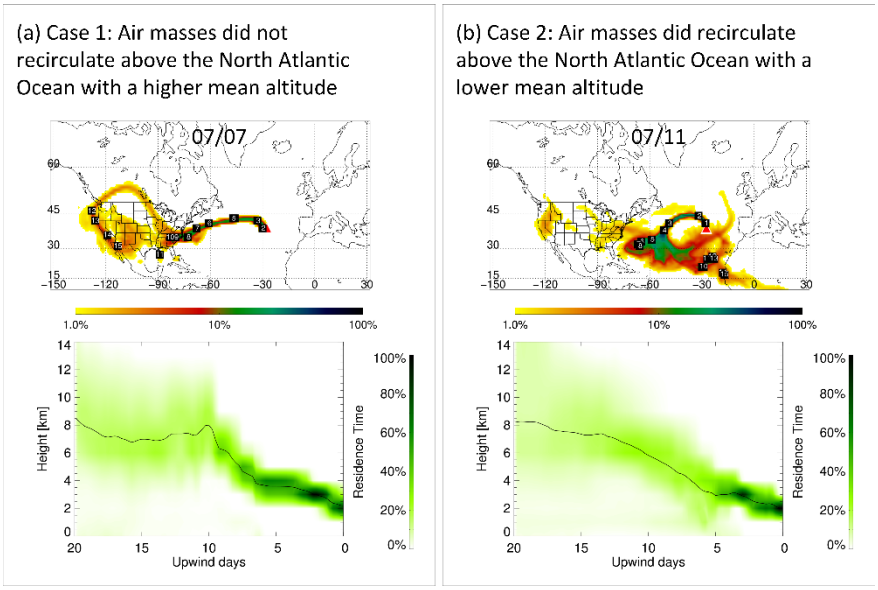

Figure 1. Representative FLEXPART back trajectories of air masses (top panel) and daily vertical distribution of retroplumes (lower panel) for two cases of transport patterns: (a) Case 1, where air masses did not recirculate above the North Atlantic Ocean and had a higher average height (07/07/2017); (b) Case 2, where air masses did recirculate above the North Atlantic Ocean with a lower mean height (07/11/2017).

The black labels with white numbers on the map views indicate the approximate locations of the center of the plume and the corresponding upwind days. Residence time is color-coded by logarithmic and linear grades in the map and vertical views, respectively, representing the ratios to each view's maximal integrated residence times. The solid black lines in the vertical views show the average height of retroplume air masses during the transport period.

3.2. Chemical composition of individual particle

Details of the samples' chemically resolved size distribution have been discussed by Cheng et al., 2022. Briefly, carbonaceous (OC+CNO) (~30-69% by number fraction), Na-rich (~8.8 to 31.6 % by number fraction), and Na-rich with S (~5.2 to 31.5 %) particles are three major particle types in our samples. The source of carbonaceous particles is long-range transported anthropogenic and wildfire emissions and new particle formations in the FT (Bianchi et al., 2016; Cheng et al., 2022). Na-rich with S particles might be products of aqueous-phase processing (i.e., fog and cloud processing). Relatively small Na-rich particles (<0.6 μm) might serve as sulfate nuclei, and large Na-rich particles (>0.6 μm) might serve as condensation nuclei of gaseous hydrogen sulfate (Ervens et al., 2011; Kim et al., 2019; Lee et al., 2012, 2011; Levin and Cotton, 2009; Sorooshian et al., 2007; Yu et al., 2005; Zhou et al., 2019). Moreover, our elemental composition retrieved from CCSEM-EDX analysis shows that sea salt and sea salt with sulfate particles are highly aged due to long atmospheric aging time during long-range transport (Section S2 in SI), suggesting these particles might be internally mixed (Laskin et al., 2012).

3.3. Mixing state of particles

Figure 2 shows the mixing state diagram for all samples (a), histograms of D_i, and area equivalent diameters for particles collected on stage 3 (S3-1 to S3-4) (b) and stage 4 (S4-1 to S4-4) (c). Histograms of D_i values for each sample are reported in Figure S5. Figure 2(a) illustrates the relationship between D_α, D_γ, and χ, and their values are listed in Table S2. Dα is smaller than Dγ for all samples, suggesting less inter-particle diversity than diversity between samples, and all samples do not have identical mass fractions (Riemer and West, 2013). The D_α and D_γ range from 1.4-2.8 and 1.5-3.8 (see Table S2), suggesting that χ is almost entirely determined by C, N, and O since these three elements dominate the mass of the individual particles and the bulk samples (Fraund et al., 2017). All samples have values of χ between 53% and 87%, indicating that the particle population were considerably internally mixed as a result of the atmospheric aging process (Riemer and West, 2013). This finding is consistent with direct observations of ESEM images and TEM images (Cheng et al., 2022) and scanning transmission X-ray microscopy (STXM) carbon speciation maps (Figure S6). These results also support our assumption that particles are internally and homogeneously mixed in calculating $\kappa_{\text{CCSEM-EDX}}$. Moreover, Ching et al., 2017 show that the mixing state is not critical for CCN prediction when $\chi > 0.75$. Thus, offline CCN prediction in this study might not be impacted by the mixing state. The variations in χ between the samples collected on stages 3 and 4 are small due to low variability in D_α and D_γ. Moreover, χ values for samples from stage 4 are higher than those from stage 3 due to a narrow spread in D_α and D_γ, suggesting larger particles were fresher. These relatively fresher particles might come from the boundary layer (Knopf et al., 2022), and smaller particles might be more aged due to longer lifetime and/or new particle formation in the FT (Bianchi et al., 2016; Rose et al., 2017). The discrepancy in χ of stage 3 and stage 4 particles suggests that χ might be size-dependent and larger particles have a larger variation in χ. This could also be attributed to the higher diversity in the sources during June 2017 (Cheng et al., 2022). Moreover, based

on the FLEXPART CO aging simulations, stage 4 samples have longer atmospheric aging time, suggesting that longer atmospheric aging time might make individual aerosols more homogeneous. This also explains the relatively low χ value of S4-4 than that of other samples from stage 4 since S4-4 has CO aging time of ~11.3 days, lower than others. Furthermore, Cheng et al., 2022 have shown that stage 4 samples have a high abundance of liquid-like particles, which promote faster diffusion and mixing of species in the aerosol, making aerosol population more internally mixed (Riemer et al., 2019; Sharma et al., 2018). A similar observation was reported by (Fraund et al., 2017) on samples collected during the Green Ocean Amazon (GoAmazon2014/5) field campaign conducted in the dry season of 2014 and by O'Brien et al., 2015 based on a field study near the Sierra Nevada Mountains during June 27 and 28, 2010, where more aged particles had smaller variation and larger value of χ.

Figures 2(b) and (c) show an overall trend of increasing average D_i with increasing area equivalent diameter, which has also been reported by (Fraund et al., 2017). O'Brien et al., 2015 also reported a similar trend when using STXM-NEXAFS to probe the mixing state of organic and inorganic. Moreover, particles collected on stage 3 show greater D_i due to a higher fraction of inorganic species and possibly lower degree of atmospheric aging. A higher fraction of inorganics increases individual particle and particle population elemental diversity, while aging makes particles more homogeneous. These two conclusions were also consistent in each sample, but the spread of D_i varied with each sample. As shown in Figure S5, the spread of D_i for S3-2 is wide, while the spread of S4-1 and S4-2 is much narrower. This is also observed in the 2-D histogram plotted for each data set.

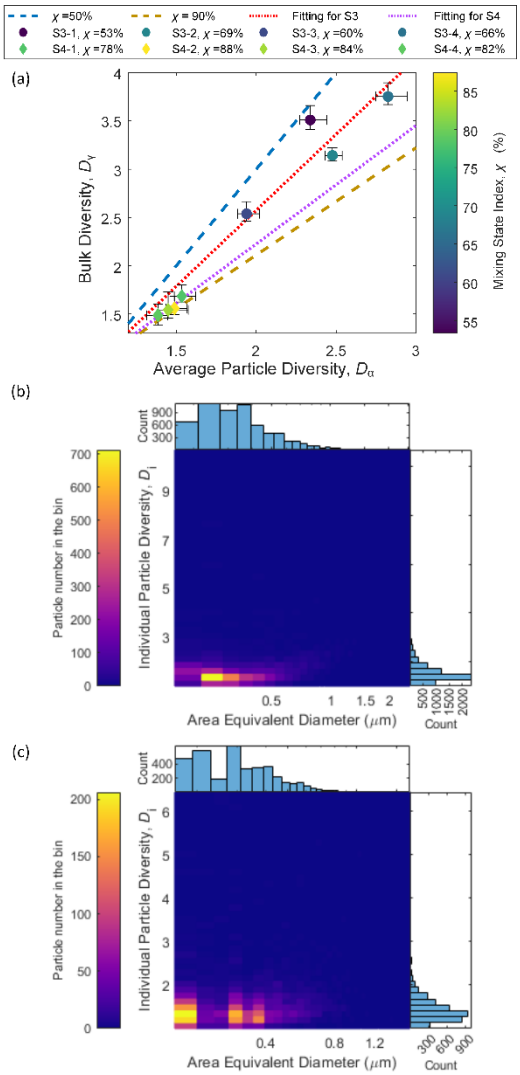

Figure 2. (a) Mixing state diagram showing the average particle diversity (D_α) and bulk diversity (D_γ). Each symbol is colored by its mixing state index (χ). The error bar represents the range of uncertainties stemming from particle aspect ratio distribution. The positive and negative error bars of D_α and D_γ are derived from the upper and lower limit of the aspect ratio, respectively. The red dash-dotted line is the linear fitting for stage 3 samples (D_γ = 1.238 D_α - 0.138, R^2 = 0.8967), and the brown dash-dotted line is the linear fitting for stage 4 samples (D_γ = 1.082 D_α - 0.059, R^2 = 0.9393). (b) and (c) Histograms of

individual particle diversity (D_i) and area equivalent diameter values for Stage 3 samples (S3-1 to S3-4, 50% cutoff diameter is 150 nm) and for Stage 4 samples (S4-1 to S4-4, 50% cutoff diameter is 50 nm). Colorbars in Figures 2 (b) and (c) represent the number of bins.

3.4. Evaluating CCN activity of mixed organic-inorganic particles

3.4.1. miniCCNC-derived hygroscopicity parameter (κ_{CCNC})

Figure 3 shows temporal CCN concentration (a), CCN fraction (CCN concentration/total particle concentration) (b), activation dry diameter ($D_{act,d}$, above which all of the particles activate into CCN under the assumption of an internally mixed particle population) (c), miniCCNC measurements derived κ_{CCNC} values (d), and violin plot of the κ_{CCNC} values at 10 different SS ratios (e) from July 5th, 2017 to July 21st, 2017. The solid black lines in Figure 3 (a-d) represent averages across the different SS ratios. Only two samples for offline analysis (narrow grey-shaded areas) (S4-1 and S4-2) overlapped with the CCN measurements. As shown in Figure 3 (a-c), at the same time, a higher SS led to higher CCN and CCN fraction and a lower $D_{act,d}$, which is expected since, at higher SS, small particles can also activate (Petters and Kreidenweis, 2007). The CCN, CCN fraction, and $D_{act,d}$ changes for increasing SS are larger when SS increases from 0.1% to 0.32% than when SS is above 0.32%. This is due to smaller and less hygroscopic particles starting to activate at higher SS, reducing the average κ value based on the CCN activation theory. For example, sample S4-2 has a higher fraction of hydrophilic species (sea salt and sea salt with sulfate) and a lower fraction of hydrophobic species (e.g., OC) than S4-1, resulting in S4-2 having higher κ_{CCNC} values when SS is less than 0.32% and lower κ_{CCNC} values when SS is higher than 0.32%. This finding is further confirmed by the κ_{CCNC} trend shown in Figures 3 (d) and (e), which show

the mean κ_{CCNC} value first increases from 0.17 to 0.45 when SS increases from 0.1% to 0.32%, then starts to decrease slightly to 0.39 for SS increase to 0.56%. This phenomenon is due to the fact that ambient particles are a complex mixture of species with different κ values which have different critical SS ratios, and their chemical composition is size-depended (Liu et al., 2018; Petters and Kreidenweis, 2007; Zhao et al., 2015). The dependence of κ_{CCNC} with SS that we measured is consistent with our mixing state index (χ) value (~53-87%), indicating a non-homogeneous aerosol population. Therefore, we acknowledge that the homogenously internal mixing assumption is required for the application of κ-Köhler theory and its application to calculate κ for both homogenously mixed and not homogenously mixed particles might introduce bias in the results. A similar trend in κ_{CCNC} with increasing SS has been reported by Gaston et al., 2018 and Royer et al., 2023. The κ_{CCNC} values at each SS ratio are highly variable due to the low particle concentrations in the free troposphere and infrequent high CCN concentration plume and plume from different sources that arrived at the site during the sampling period, resulting in aerosols with variable properties. Moreover, the site also infrequently receives highly hygroscopic particles (e.g., sea salt) plumes, leading to extreme values of κ_{CCNC}.

The range of κ_{CCNC} values at each SS (0.17±0.09 – 0.44±0.16, see Table S3) is in good agreement with literature reported κ values of particles collected over the North Atlantic Ocean and overall in the free troposphere (0.05-0.88) (Kammermann et al., 2010; Pringle et al., 2010; Roberts et al., 2010; Schulze et al., 2020; Zheng et al., 2020). July 11th to 18th have lower average $D_{act,d}$ and higher κ_{CCNC} overall SS ratios (~90.5±46.1 and ~0.45±0.16, respectively, where the value after the ± represents one standard deviation) than other days (~105.1±53.8 and ~0.32±0.12, respectively). Based on the FLEXPART simulations (Figure S1 and S2), air masses that arrived at OMP these days likely had higher contributions from sea salt particles, which are very hygroscopic. Moreover, from July 20th to July 22nd, $D_{act,d}$ and κ_{CCNC} values

(~111.5±60.0 nm and ~0.29±0.34, respectively) are more variable (higher standard deviation) than those for other days across all SS ratios (~98.0±47.7 nm and ~0.35±0.38, respectively). It has been shown in Section 3.1 that these days had a higher CO contribution from wildfires. Thus, we suggest that wildfires might lead to particles with more complex hygroscopicity, which is worth further study. This complex hygroscopicity might be partly due to the diversity of particle types generated during the wildfire, mostly carbonaceous with a wide variety of chemical compositions, leading to variable hygroscopicities.

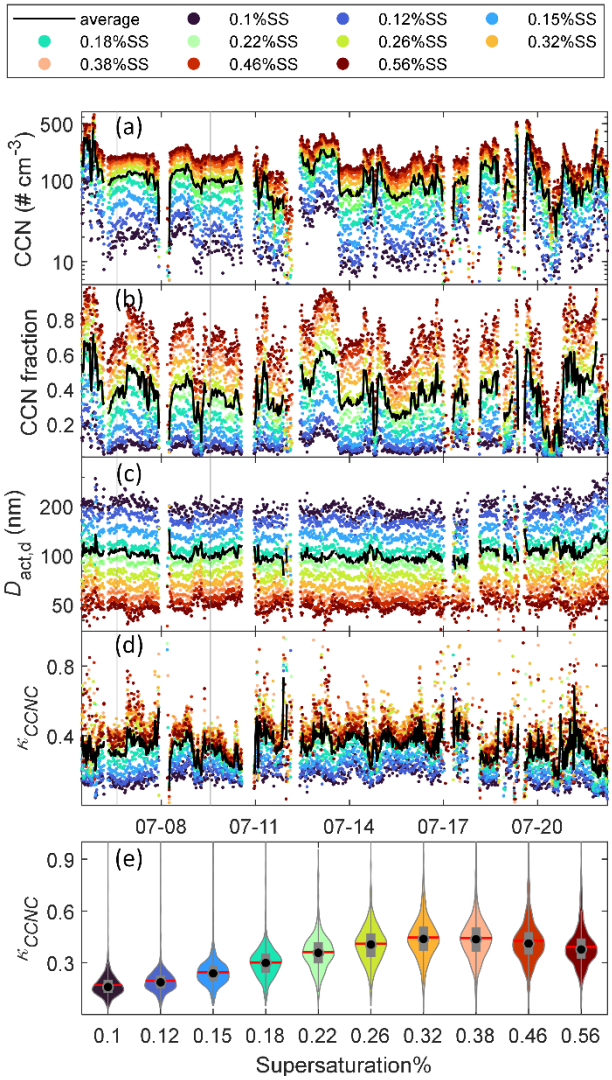

Figure 3. Time series of (a) CCN concentration, (b) CCN fraction (CCN concentration/total particle concentration), (c) activation dry diameter ($D_{act,d}$, above which all of the particles activate), and (d) hygroscopicity parameter (κ_{CCNC}), from July 5th to July 21st, 2017. The solid black lines in (a-d) are the averages across all SS (SS) ratios, and the narrow gray shaded areas represent the sample collection periods for S4-1(40 minutes) and S4-2 (70 minutes) (50% cutoff diameter is 150 nm). (e) Violin plots of κ_{CCNC} values in ten SS bins. The red lines indicate the means, the black dots are the medians, the gray rectangles are the interquartile ranges, the gray verticle lines are the 95% confidence intervals, and the violin-shaded areas show the data distribution.

3.4.2. Individual particle chemical composition derived hygroscopicity parameter ($\kappa_{CCSEM\text{-}EDX}$)

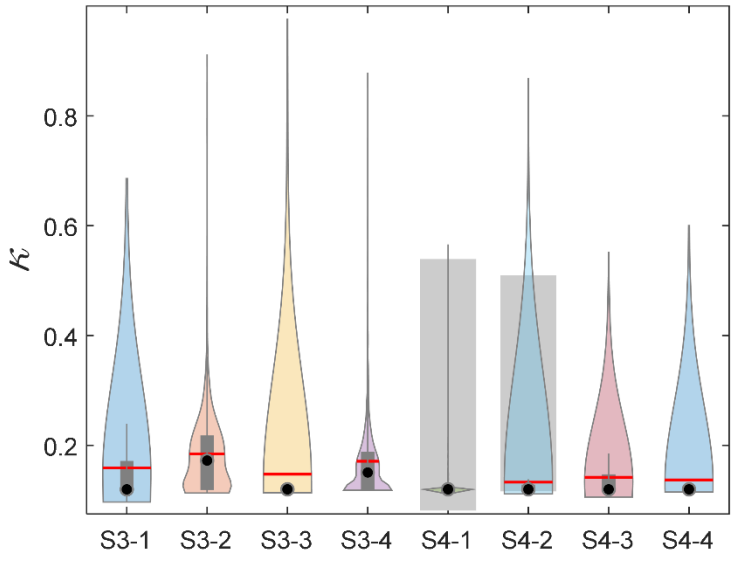

Figure 4. Violin plot of κ values derived from the CCSEM-EDX chemical composition analysis. The red lines indicate the means, the black dots are the medians, the gray rectangles are the interquartile ranges,

the gray verticle lines are the 95% confidence intervals, and the violin-shaded areas show the data distribution. The large shaded areas represent the range of κ values derived from CCN measurements. S3-1 to S3-4 were collected on stage 3 (50% cutoff diameter: 150 nm), and S4-1 to S4-4 were collected on stage 4 (50% cutoff diameter: 50 nm).

The mass-weighted average κ values ($\bar{\kappa}_{\mathrm{CCSEM\text{-}EDX}}$) and their uncertainties range derived from CCSEM-EDX chemical composition are listed in Table S2, and their distributions are shown in Figure 4 in the form of violin plots. The predicted $\kappa_{\mathrm{CCSEM\text{-}EDX}}$ values ranged from 0.10-0.98, in good agreement with literature reported κ values for FT particles and particles collected over the North Atlantic Ocean (0.05-0.88) (Kammermann et al., 2010; Pringle et al., 2010; Roberts et al., 2010; Schulze et al., 2020; Zheng et al., 2020). Predicted $\kappa_{\mathrm{CCSEM\text{-}EDX}}$ values have a wide range due to variations in individual particles' elemental composition and morphology. Stage 3 samples (S3-1 to S3-4) have slightly higher average $\kappa_{\mathrm{CCSEM\text{-}EDX}}$ values than stage 4 samples (S4-1 to S4-4) due to the larger 50% cutoff diameter of stage 3 than stage 4 (150 vs. 50 nm, respectively). These larger particles contain a higher volume fraction of sea salts and sulfates (see Figure S7), which are hydrophilic and have larger sizes to be better activated as CCN. The shaded large ractangle areas in Figure 4 represent the range of κ_{CCNC} values during the sampling periods of S4-1 and S4-2 (κ_{CCNC} ranges from 0.08 to 0.54 and 0.15 to 0.48, respectively). The $\bar{\kappa}_{\mathrm{CCSEM\text{-}EDX}}$ values for S4-1 and S4-2 are 0.14±0.03 and 0.15±0.04, respectively, within the lower range of κ_{CCNC} (SS < 0.15%). The primary reason is that S4-1 and S4-2 were collected on stage 4, whose cutoff diameter is 50 nm, smaller than the $D_{act,d}$ from the miniCCNC measurements until SS reached ~0.46%. Moreover, particle volume derived from CCSEM-EDX measurements might be lower than the actual particles in the atmosphere due to liquid water and volatile species losses inside the SEM chamber. Therefore, particles

in S4-1 and S4-2 might not activate as CCN efficiently until the SS is larger than 0.46%. On the other hand, the $\kappa_{CCSEM\text{-}EDX}$ value of more than 99% of particles in S4-1 and S4-2 were within the range of κ_{CCNC} values during the sampling periods, suggesting offline CCSEM-EDX method could be a potentially valuable tool to predict individual particle's κ values.

Besides, discrepancies between κ_{CCNC} and $\kappa_{CCSEM\text{-}EDX}$ values might partially arise from limitations in measurement techniques and the associated biases and uncertainties. In this study, we could underestimate the κ value of carbonaceous species, which can range over an order of magnitude due to variable carbon chain length and functional groups (Petters et al., 2017) and oxidation levels (Chang et al., 2010; Lambe et al., 2011). We have shown in Cheng et al., 2022 that our samples are highly aged and potentially oxidized during long-range transport. An improved estimate of the κ values for carbonaceous species could be obtained from mass spectrometry since the κ value of carbonaceous species is positively correlated with the O/C ratio (Lambe et al., 2011). Moreover, we might overestimate the carbonaceous weight fraction since we assume all C belongs to organics, neglecting C, N, and O inorganic species (e.g., CO_3^{2-}). Furthermore, we might underestimate the weight fraction of sea salt species by not including some elemental fractions (e.g., metals). The interactions between species can alter the κ values. For instance, the CCN activation of sea salt particles can be enhanced by surfactant coatings (e.g., oleic acid) due to the reduction of the surface tension (Bramblett and Frossard, 2022; Forestieri et al., 2018; Nguyen et al., 2017). However, we cannot estimate these interactions due to a lack of molecular data. Last, due to the limited instrument available time and limitation and challenges of access to the OMP, we have only two samples during the CCN measurements, making the comparison less statistically significant. Therefore, to better understand the effects of chemical composition and

mixing state on aerosol CCN activities, it is critical to collect more data sets and samples at remote sites and to apply mass spectrometry analyses to constrain the organic composition of particles better.

4. Conclusions.

This study investigated mixing state and CCN activities of free tropospheric particles. Multi-modal micro-spectroscopy techniques (CCSEM-EDX and STXM-NEXAFS) were used to probe the chemical composition, mixing state, and hygroscopicity parameters (κ) of these free-tropospheric, long-range transported particles. κ derived from miniCCNC measurements (κ_{CCNC}), ranging from 0.17±0.09 to 0.44±0.16, is within the range reported in the literature for particles collected over the North Atlantic Ocean. Combining miniCCNC measurements with FLEXPART simulation, we found air masses with lower mean height and recirculating over the North Atlantic Ocean for a longer period present higher mean κ_{CCNC} values due to the contribution of sea spray aerosols (e.g., sea salt). CCSEM-EDX analysis indicated that all samples were dominated by carbonaceous aerosols (~30-69% by number) but still contained a substantial fraction of sea salt particles (~8.8 to 31.6 % by number) and sea salt with sulfate (~5.2 to 31.5 %) particles since the air masses were transported over the North Atlantic Ocean. The mixing state index (χ) analysis revealed that all samples were internally mixed particle population (0.53-0.87), but larger particles (stage 3 samples) have lower values (0.53-0.69) in the mixing stage index than smaller particles (stage 4 samples) (0.78-0.87), suggesting that the mixing state depends on size with large particles being fresher. Our estimated $\kappa_{CCSEM\text{-}EDX}$ values are within the lower range of the measured κ_{CCNC} values, suggesting that CCSEM-EDX combined with phase state measurements can be used to predict κ values of ambient particles. However, we still found a discrepancy between $\kappa_{CCSEM\text{-}EDX}$ and κ_{CCN}, which might be due to 1) differences in particle size ranges between the stages of the impactor and the CCN counter; 2)

lack of detailed knowledge on the molecular composition of organics; 3) lack of detailed knowledge on the mass fraction and spatial distribution (single particle mixing state) of different species within each particle which hampers our ability to account for interactions among different species; and 4) limited number of samples. The first aspect can be resolved by collecting a wider size range of particles in the future. The second can be improved by applying molecular analysis using mass spectrometry. The third can be addressed by combining higher spatial resolution CCSEM-EDX with STXM-NEXAFS measurements on the same particles to obtain single-particle molecular information. The last limitation could be improved by collecting and analyzing more samples; however, this limitation should also be put in the context of the remoteness and difficult access to OMP, which makes a collection of samples more challenging than at most other atmospheric monitoring sites but concurrently provides opportunities for more unique sampling.

Our results are critical for understanding the CCN properties when deployment of online CCN and chemical composition measurement instruments (e.g., CCNC and AMS) is not feasible (e.g., onboard tethered balloon system) to study aerosol vertical distribution or at remote sites that do not have CCN data but have samples for single particle or off-line chemical analysis. Moreover, our study provides opportunities for probing ambient particles' CCN activities using chemical composition data (e.g., from mass spectrometry) without CCNC measurements. Widespread estimates of CCN activities are crucial for climate models to predict the indirect radiative forcing of ambient particles based on the particle's chemical composition. Moreover, our offline single-particle method provides κ value at the individual particle level, which can help reduce uncertainties associated with the particle-resolved mixing state in the climate model predicted CCN (Fierce et al., 2013; Healy et al., 2014). Climate models typically

assume particles are homogeneously mixed and use a single κ, which might underrepresent the variation between individual particles. Future studies should aim to develop a parameterization to incorporate the mixing state index in aerosol population average κ calculation based on individual particle measurements. Finally, our study underscores the urgent need to collect additional field data on FT aerosols to improve our understanding of aerosol-cloud interactions and enhance the accuracy of climate models. Our proposed method works well with FT particles since they are usually long-range transported and well-mixed. However, the proposed method might incorporate relatively higher uncertainties for relatively less atmospheric aged (e.g., urban and fresh biomass burning particles) particles where particles might have different morphological configurations (e.g., core-shell and partially engulfed) (Lingaswamy et al., 2022; Unga et al., 2018). Future studies should investigate the spatial distribution of different species in the particles to improve the hygroscopicity parameter estimation.

Acknowledgments.

A portion of this research was performed on a project award (10.46936/lser.proj.2019.50835/60000118) from the Environmental Molecular Sciences Laboratory (EMSL). EMSL is a US Department of Energy (DOE) Office of Science User Facility sponsored by the Biological and Environmental Research (BER) program under Contract No. DE-AC05-76RL01830. STXM/NEXAFS analysis was perfromed at the Advanced Light Source (beamline 5.3.2.2) at Lawrence Berkeley National Laboratory. ALS is supported by the Office of Basic Energy Sciences of the U.S. DOE under Contract No. DE-AC02- 05CH11231. We thank support from the U.S. DOE-BER, Atmospheric System Research. Some of the sample collection anddata analysis were supported with funding from NSF (AGS-1110059), DOE (DE-SC0006941 and DE-SC0020053), and NASA's Earth and Space Science Graduate Fellowships (NNX12AN97H, and

NNX13AN68H). We thank the Regional Government of the Azores for providing logistic support for the operation of the site through the Regional Secretary for Science and the Pico Island Natural Park. We thank Andrea Baccarini, Mike Dziobak, Detlev Helmig, Jacques Huber, Sumit Kumar, Kendra Wright, Stefano Viviani, and Oliver Welz, for their help in the field. Aerosol measurements in 2017 were supported by the German Science Foundation (Deutsche Forschungsgemeinschaft, DFG) under SI 1543/4-1, WE 2757/2-1, and HE 6770/2-1.

Reference:

Allen, S., Allen, D., Baladima, F., Phoenix, V.R., Thomas, J.L., Le Roux, G., Sonke, J.E., 2021. Evidence of free tropospheric and long-range transport of microplastic at Pic du Midi Observatory. Nat. Commun. 12. https://doi.org/10.1038/s41467-021-27454-7

Altaf, M.B., Dutcher, D.D., Raymond, T.M., Freedman, M.A., 2018. Effect of Particle Morphology on Cloud Condensation Nuclei Activity. ACS Earth Sp. Chem. 2, 634–639. https://doi.org/10.1021/acsearthspacechem.7b00146

Baustian, K.J., Cziczo, D.J., Wise, M.E., Pratt, K.A., Kulkarni, G., Hallar, A.G., Tolbert, M.A., 2012. Importance of aerosol composition , mixing state , and morphology for heterogeneous ice nucleation : A combined field and laboratory approach. J. Geophys. Res 117, D06217. https://doi.org/10.1029/2011JD016784

Bellouin, N., Quaas, J., Gryspeerdt, E., Kinne, S., Stier, P., Watson-Parris, D., Boucher, O., Carslaw, K.S., Christensen, M., Daniau, A.L., Dufresne, J.L., Feingold, G., Fiedler, S., Forster, P., Gettelman, A., Haywood, J.M., Lohmann, U., Malavelle, F., Mauritsen, T., McCoy, D.T., Myhre, G., Mülmenstädt, J.,

Neubauer, D., Possner, A., Rugenstein, M., Sato, Y., Schulz, M., Schwartz, S.E., Sourdeval, O., Storelvmo, T., Toll, V., Winker, D., Stevens, B., 2020. Bounding Global Aerosol Radiative Forcing of Climate Change. Rev. Geophys. 58, 1–45. https://doi.org/10.1029/2019RG000660

Bhattu, D., Tripathi, S.N., 2015. CCN closure study: Effects of aerosol chemical composition and mixing state. J. Geophys. Res. Atmos. 120, 766–783. https://doi.org/10.1002/2014JD021978

Bhattu, D., Tripathi, S.N., Chakraborty, A., 2016. Deriving aerosol hygroscopic mixing state from size-resolved CCN activity and HR-ToF-AMS measurements. Atmos. Environ. 142, 57–70. https://doi.org/10.1016/j.atmosenv.2016.07.032

Bianchi, F., Tröstl, J., Junninen, H., Frege, C., Henne, S., Hoyle, C.R., Molteni, U., Herrmann, E., Adamov, A., Bukowiecki, N., Chen, X., Duplissy, J., Gysel, M., Hutterli, M., Kangasluoma, J., Kontkanen, J., Kürten, A., Manninen, H.E., Münch, S., Peräkylä, O., Petäjä, T., Rondo, L., Williamson, C., Weingartner, E., Curtius, J., Worsnop, D.R., Kulmala, M., Dommen, J., Baltensperger, U., 2016. New particle formation in the free troposphere: A question of chemistry and timing. Science (80-.). 352, 1109–1112. https://doi.org/10.1126/science.aad5456

Bond, T.C., Doherty, S.J., Fahey, D.W., Forster, P.M., Berntsen, T., DeAngelo, B.J., Flanner, M.G., Ghan, S., Kärcher, B., Koch, D., Kinne, S., Kondo, Y., Quinn, P.K., Sarofim, M.C., Schultz, M.G., Schulz, M., Venkataraman, C., Zhang, H., Zhang, S., Bellouin, N., Guttikunda, S.K., Hopke, P.K., Jacobson, M.Z., Kaiser, J.W., Klimont, Z., Lohmann, U., Schwarz, J.P., Shindell, D., Storelvmo, T., Warren, S.G., Zender, C.S., 2013. Bounding the role of black carbon in the climate system: A scientific assessment. J. Geophys. Res. Atmos. 118, 5380–5552. https://doi.org/10.1002/jgrd.50171

Bondy, A.L., Bonanno, D., Moffet, R.C., Wang, B., Laskin, A., Ault, A.P., 2018. The diverse chemical mixing

state of aerosol particles in the southeastern United States. Atmos. Chem. Phys. 18, 12595–12612. https://doi.org/10.5194/acp-18-12595-2018

Bramblett, R.L., Frossard, A.A., 2022. Constraining the Effect of Surfactants on the Hygroscopic Growth of Model Sea Spray Aerosol Particles. J. Phys. Chem. A 126, 8695–8710. https://doi.org/10.1021/acs.jpca.2c04539

Chang, R.Y.W., Slowik, J.G., Shantz, N.C., Vlasenko, A., Liggio, J., Sjostedt, S.J., Leaitch, W.R., Abbatt, J.P.D., 2010. The hygroscopicity parameter (κ) of ambient organic aerosol at a field site subject to biogenic and anthropogenic influences: Relationship to degree of aerosol oxidation. Atmos. Chem. Phys. 10, 5047–5064. https://doi.org/10.5194/acp-10-5047-2010

Cheng, Z., Morgenstern, M., Zhang, B., Fraund, M., Lata, N.N., Brimberry, R., Marcus, M.A., Mazzoleni, L., Fialho, P., Henning, S., Wehner, B., Mazzoleni, C., China, S., 2022. Particle phase-state variability in the North Atlantic free troposphere during summertime is determined by atmospheric transport patterns and sources. Atmos. Chem. Phys. 22, 9033–9057. https://doi.org/10.5194/acp-22-9033-2022

Cheng, Z., Sharma, N., Tseng, K.-P., Kovarik, L., China, S., 2021. Direct observation and assessment of phase states of ambient and lab-generated sub-micron particles upon humidification. RSC Adv. 11, 15264–15272. https://doi.org/10.1039/d1ra02530a

China, S., Alpert, P.A., Zhang, B., Schum, S., Dzepina, K., Wright, K., Owen, R.C., Fialho, P., Mazzoleni, L.R., Mazzoleni, C., Knopf, D.A., 2017. Ice cloud formation potential by free tropospheric particles from long-range transport over the Northern Atlantic Ocean. J. Geophys. Res. Atmos. 122, 3065–3079. https://doi.org/10.1002/2016JD025817

China, S., Mazzoleni, C., Gorkowski, K., Aiken, A.C., Dubey, M.K., 2013. Morphology and mixing state of individual freshly emitted wildfire carbonaceous particles. Nat. Commun. 4, 1–7. https://doi.org/10.1038/ncomms3122

China, S., Scarnato, B., Owen, R.C., Zhang, B., Ampadu, M.T., Kumar, S., Dzepina, K., Dziobak, M.P., Fialho, P., Perlinger, J.A., Hueber, J., Helmig, D., Mazzoleni, L.R., Mazzoleni, C., 2015. Morphology and mixing state of aged soot particles at a remote marine free troposphere site: Implications for optical properties. Geophys. Res. Lett. 42, 1243–1250. https://doi.org/10.1002/2014GL062404

Ching, J., Adachi, K., Zaizen, Y., Igarashi, Y., Kajino, M., 2019. Aerosol mixing state revealed by transmission electron microscopy pertaining to cloud formation and human airway deposition. npj Clim. Atmos. Sci. 2, 1–7. https://doi.org/10.1038/s41612-019-0081-9

Ching, J., Fast, J., West, M., Riemer, N., 2017. Metrics to quantify the importance of mixing state for CCN activity. Atmos. Chem. Phys. 17, 7445–7458. https://doi.org/10.5194/acp-17-7445-2017

Clarke, A.D., Freitag, S., Simpson, R.M.C., Hudson, J.G., Howell, S.G., Brekhovskikh, V.L., Campos, T., Kapustin, V.N., Zhou, J., 2013. Free troposphere as a major source of CCN for the equatorial pacific boundary layer: Long-range transport and teleconnections. Atmos. Chem. Phys. 13, 7511–7529. https://doi.org/10.5194/acp-13-7511-2013

De Wekker, S.F.J., Kossmann, M., 2015. Convective boundary layer heights over mountainous terrain—A review of concepts. Front. Earth Sci. 3, 1–22. https://doi.org/10.3389/feart.2015.00077

Dzepina, K., Mazzoleni, C., Fialho, P., China, S., Zhang, B., Owen, R.C., Helmig, D., Hueber, J., Kumar, S., Perlinger, J.A., Kramer, L.J., Dziobak, M.P., Ampadu, M.T., Olsen, S., Wuebbles, D.J., Mazzoleni, L.R., 2015. Molecular characterization of free tropospheric aerosol collected at the Pico Mountain

Observatory: A case study with a long-range transported biomass burning plume. Atmos. Chem. Phys. 15, 5047–5068. https://doi.org/10.5194/acp-15-5047-2015

Ervens, B., Turpin, B.J., Weber, R.J., 2011. Secondary organic aerosol formation in cloud droplets and aqueous particles (aqSOA): A review of laboratory, field and model studies. Atmos. Chem. Phys 11, 11069–11102. https://doi.org/10.5194/acp-11-11069-2011

Fan, J., Wang, Y., Rosenfeld, D., Liu, X., 2016. Review of aerosol-cloud interactions: Mechanisms, significance, and challenges. J. Atmos. Sci. 73, 4221–4252. https://doi.org/10.1175/JAS-D-16-0037.1

Fan, X., Liu, J., Zhang, F., Chen, L., Collins, D., Xu, W., Jin, X., Ren, J., Wang, Y., Wu, H., Li, S., Sun, Y., Li, Z., 2020. Contrasting size-resolved hygroscopicity of fine particles derived by HTDMA and HR-ToF-AMS measurements between summer and winter in Beijing: The impacts of aerosol aging and local emissions. Atmos. Chem. Phys. 20, 915–929. https://doi.org/10.5194/acp-20-915-2020

Fierce, L., Riemer, N., Bond, T.C., 2013. When is cloud condensation nuclei activity sensitive to particle characteristics at emission? J. Geophys. Res. Atmos. 118, 13,476-13,488. https://doi.org/10.1002/2013JD020608

Fofie, E.A., Donahue, N.M., Asa-Awuku, A., 2018. Cloud condensation nuclei activity and droplet formation of primary and secondary organic aerosol mixtures. Aerosol Sci. Technol. 52, 242–251. https://doi.org/10.1080/02786826.2017.1392480

Forestieri, S.D., Staudt, S.M., Kuborn, T.M., Faber, K., Ruehl, C.R., Bertram, T.H., Cappa, C.D., 2018. Establishing the impact of model surfactants on cloud condensation nuclei activity of sea spray aerosol mimics. Atmos. Chem. Phys. 18, 10985–11005. https://doi.org/10.5194/acp-18-10985-2018

Forster, P., Alterskjaer, K., Smith, C., Colman, R., Damon Matthews, H., Ramaswamy, V., Storelvmo, T., Armour, K., Collins, W., Dufresne, J., Frame, D., Lunt, D., Mauritsen, T., Watanabe, M., Wild, M., Zhang, H., Masson-Delmotte, V., P. Zhai, Pirani, A., Connors, S., Péan, C., Berger, S., Caud, N., Chen, Y., Goldfarb, L., Gomis, M., Huang, M., Leitzell, K., Lonnoy, E., Matthews, J., Maycock, T., Waterfield, T., Yelekçi, O., Yu, R., Zhou, B., 2021. The Earth's Energy Budget, Climate Feedbacks, and Climate Sensitivity. In Climate Change 2021: The Physical Science Basis. Contribution of Working Group I to the Sixth Assessment Report of the Intergovernmental Panel on Climate Change, Cambridge University Press, Cambridge, United Kingdom and New York, NY, USA. https://doi.org/10.1017/9781009157896.009.923

Fraund, M., Pham, D.Q., Bonanno, D., Harder, T.H., Wang, B., Brito, J., de Sá, S.S., Carbone, S., China, S., Artaxo, P., Martin, S.T., Pöhlker, C., Andreae, M.O., Laskin, A., Gilles, M.K., Moffet, R.C., 2017. Elemental Mixing State of Aerosol Particles Collected in Central Amazonia during GoAmazon2014/15. Atmosphere (Basel). 8. https://doi.org/10.3390/atmos8090173

Gaston, C.J., Cahill, J.F., Collins, D.B., Suski, K.J., Ge, J.Y., Barkley, A.E., Prather, K.A., 2018. The cloud nucleating properties and mixing state of marine aerosols sampled along the Southern California coast. Atmosphere (Basel). 9. https://doi.org/10.3390/atmos9020052

Hammer, E., Gysel, M., Roberts, G.C., Elias, T., Hofer, J., Hoyle, C.R., Bukowiecki, N., Dupont, J.-C., Burnet, F., Baltensperger, U., Weingartner, E., 2014. Size-dependent particle activation properties in fog during the ParisFog 2012/13 field campaign. Atmos. Chem. Phys. 14, 10517–10533. https://doi.org/10.5194/acp-14-10517-2014

Hatch, C.D., Gierlus, K.M., Schuttlefield, J.D., Grassian, V.H., 2008. Water adsorption and cloud

condensation nuclei activity of calcite and calcite coated with model humic and fulvic acids. Atmos. Environ. 42, 5672–5684. https://doi.org/10.1016/j.atmosenv.2008.03.005

Healy, R.M., Evans, G.J., Murphy, M., Jurányi, Z., Tritscher, T., Laborde, M., Weingartner, E., Gysel, M., Poulain, L., Kamilli, K.A., Wiedensohler, A., O'Connor, I.P., McGillicuddy, E., Sodeau, J.R., Wenger, J.C., 2014. Predicting hygroscopic growth using single particle chemical composition estimates. J. Geophys. Res. Atmos. 119, 9567–9577. https://doi.org/10.1002/2014JD021888

Honrath, R.E., Owen, R.C., Val Martín, M., Reid, J.S., Lapina, K., Fialho, P., Dziobak, M.P., Kleissl, J., Westphal, D.L., 2004. Regional and hemispheric impacts of anthropogenic and biomass burning emissions on summertime CO and O3 in the North Atlantic lower free troposphere. J. Geophys. Res. 109, 1–17. https://doi.org/10.1029/2004JD005147

Igel, A.L., Ekman, A.M.L., Leck, C., Tjernström, M., Savre, J., Sedlar, J., 2017. The free troposphere as a potential source of arctic boundary layer aerosol particles. Geophys. Res. Lett. 44, 7053–7060. https://doi.org/10.1002/2017GL073808

Ilotoviz, E., Ghate, V.P., Raveh-Rubin, S., 2021. The Impact of Slantwise Descending Dry Intrusions on the Marine Boundary Layer and Air-Sea Interface Over the ARM Eastern North Atlantic Site. J. Geophys. Res. Atmos. 126, e2020JD033879. https://doi.org/10.1029/2020JD033879

Jacobson, M.Z., 2001. Strong radiative heating due to the mixing state of black carbon in atmospheric aerosols. Nature 409, 695–697. https://doi.org/10.1038/35055518

Jurányi, Z., Tritscher, T., Gysel, M., Laborde, M., Roberts, G., Baltensperger, U., Weingartner, E., 2013. Hygroscopic mixing state of urban aerosol derived from size-resolved cloud condensation nuclei measurements during the MEGAPOLI campaign in Paris. Atmos. Chem. Phys. 13, 6431–6446.

https://doi.org/10.5194/acp-13-6431-2013

Kammermann, L., Gysel, M., Weingartner, E., Baltensperger, U., 2010. 13-month climatology of the aerosol hygroscopicity at the free tropospheric site Jungfraujoch (3580 m a.s.l.). Atmos. Chem. Phys. 10, 10717–10732. https://doi.org/10.5194/acp-10-10717-2010

Kawana, K., Nakayama, T., Mochida, M., 2016. Hygroscopicity and CCN activity of atmospheric aerosol particles and their relation to organics: Characteristics of urban aerosols in Nagoya, Japan. J. Geophys. Res. Atmos. 121, 4100–4121. https://doi.org/10.1002/ 2015JD023213

Kim, H., Collier, S., Ge, X., Xu, J., Sun, Y., Jiang, W., Wang, Y., Herckes, P., Zhang, Q., 2019. Chemical processing of water-soluble species and formation of secondary organic aerosol in fogs. Atmos. Environ. 200, 158–166. https://doi.org/10.1016/j.atmosenv.2018.11.062

Knopf, D.A., Alpert, P.A., Wang, B., 2018. The Role of Organic Aerosol in Atmospheric Ice Nucleation: A Review. ACS Earth Sp. Chem. 2, 168–202. https://doi.org/10.1021/acsearthspacechem.7b00120

Knopf, D.A., Charnawskas, J.C., Wang, P., Wong, B., Tomlin, J.M., Jankowski, K.A., Fraund, M., Veghte, D.P., China, S., Laskin, A., Moffet, R.C., Gilles, M.K., Aller, J.Y., Marcus, M.A., Raveh-Rubin, S., Wang, J., 2022. Micro-spectroscopic and freezing characterization of ice-nucleating particles collected in the marine boundary layer in the eastern North Atlantic. Atmos. Chem. Phys. 22, 5377–5398. https://doi.org/10.5194/acp-22-5377-2022

Koch, D., Schulz, M., Kinne, S., Mcnaughton, C., Spackman, J.R., Balkanski, Y., Bauer, S., Berntsen, T., D. Koch, M. Schulz, S. Kinne, C. McNaughton, J. R. Spackman, Y. Balkanski, S. Bauer, T. Berntsen, T. C. Bond, O. Boucher, M. Chin, A. Clarke, N. De Luca, F. Dentener, T. Diehl, O. Dubovik, R. Easter, D. W. Fahey, J. Feichter, D. Fillmore, S. Freitag, S. G, and Y.Z., 2009. Evaluation of black carbon

estimations in global aerosol models. Atmos. Chem. Phys. 79–81.

Kolb, C.E., Worsnop, D.R., 2012. Chemistry and Composition of Atmospheric Aerosol Particles. Annu. Rev. Phys. Chem. 63, 471–91. https://doi.org/10.1146/annurev-physchem-032511-143706

Kristensen, T.B., Müller, T., Kandler, K., Benker, N., Hartmann, M., Prospero, J.M., Wiedensohler, A., Stratmann, F., 2016. Properties of cloud condensation nuclei (CCN) in the trade wind marine boundary layer of the western North Atlantic. Atmos. Chem. Phys. 16, 2675–2688. https://doi.org/10.5194/acp-16-2675-2016

Lack, D.A., Cappa, C.D., 2010. Impact of brown and clear carbon on light absorption enhancement, single scatter albedo and absorption wavelength dependence of black carbon. Atmos. Chem. Phys. 10, 4207–4220. https://doi.org/10.5194/acp-10-4207-2010

Lambe, A.T., Onasch, T.B., Massoli, P., Croasdale, D.R., Wright, J.P., Ahern, A.T., Williams, L.R., Worsnop, D.R., Brune, W.H., Davidovits, P., 2011. Laboratory studies of the chemical composition and cloud condensation nuclei (CCN) activity of secondary organic aerosol (SOA) and oxidized primary organic aerosol (OPOA). Atmos. Chem. Phys. 11, 8913–8928. https://doi.org/10.5194/acp-11-8913-2011

Lance, S., Nenes, A., Medina, J., Smith, J.N., 2006. Mapping the Operation of the DMT Continuous Flow CCN Counter. Aerosol Sci. Technol. 40, 242–254. https://doi.org/10.1080/02786820500543290

Lance, S., Raatikainen, T., Onasch, T.B., Worsnop, D.R., Yu, X.Y., Alexander, M.L., Stolzenburg, M.R., McMurry, P.H., Smith, J.N., Nenes, A., 2013. Aerosol mixing state, hygroscopic growth and cloud activation efficiency during MIRAGE 2006. Atmos. Chem. Phys. 13, 5049–5062. https://doi.org/10.5194/acp-13-5049-2013

Laskin, A., Cowin, J.P., Iedema, M.J., 2006. Analysis of individual environmental particles using modern methods of electron microscopy and X-ray microanalysis. J. Electron Spectros. Relat. Phenomena 150, 260–274. https://doi.org/10.1016/j.elspec.2005.06.008

Laskin, A., Laskin, J., Nizkorodov, S.A., 2015. Chemistry of Atmospheric Brown Carbon. Chem. Rev. 115, 4335–4382. https://doi.org/10.1021/cr5006167

Laskin, A., Moffet, R.C., Gilles, M.K., Fast, J.D., Zaveri, R.A., Wang, B., Nigge, P., Shutthanandan, J., 2012. Tropospheric chemistry of internally mixed sea salt and organic particles: Surprising reactivity of NaCl with weak organic acids. J. Geophys. Res. 117, 1–12. https://doi.org/10.1029/2012JD017743

Laskin, A., Wietsma, T.W., Krueger, B.J., Grassian, V.H., 2005. Heterogeneous chemistry of individual mineral dust particles with nitric acid: A combined CCSEM/EDX, ESEM, and ICP-MS study. J. Geophys. Res. 110, D10208. https://doi.org/10.1029/2004JD005206

Lata, N.N., Zhang, B., Schum, S., Mazzoleni, L., Brimberry, R., Marcus, M.A., Cantrell, W.H., Fialho, P., Mazzoleni, C., 2021. Aerosol Composition, Mixing State, and Phase State of Free Tropospheric Particles and Their Role in Ice Cloud Formation. ACS Earth Sp. Chem. 5, 3499–3510. https://doi.org/10.1021/acsearthspacechem.1c00315

Lathem, T.L., Nenes, A., 2011. Water Vapor Depletion in the DMT Continuous-Flow CCN Chamber: Effects on Supersaturation and Droplet Growth. Aerosol Sci. Technol. 45, 604–615. https://doi.org/10.1080/02786826.2010.551146

Leck, C., Svensson, E., 2015. Importance of aerosol composition and mixing state for cloud droplet activation over the Arctic pack ice in summer. Atmos. Chem. Phys. 15, 2545–2568. https://doi.org/10.5194/acp-15-2545-2015

Lee, A.K.Y., Hayden, K.L., Herckes, P., Leaitch, W.R., Liggio, J., MacDonald, A.M., Abbatt, J.P.D., 2012. Characterization of aerosol and cloud water at a mountain site during WACS 2010: Secondary organic aerosol formation through oxidative cloud processing. Atmos. Chem. Phys 12, 7103–7116. https://doi.org/10.5194/acp-12-7103-2012

Lee, A.K.Y., Herckes, P., Leaitch, W.R., MacDonald, A.M., Abbatt, J.P.D., 2011. Aqueous OH oxidation of ambient organic aerosol and cloud water organics: Formation of highly oxidized products. Geophys. Res. Lett. 38, 2–6. https://doi.org/10.1029/2011GL047439

Levin, Z., Cotton, W.R., 2009. Aerosol Pollution Impact on Precipitation, Aerosol Pollution Impact on Precipitation: A Scientific Review. Springer Netherlands, Dordrecht. https://doi.org/10.1007/978-1-4020-8690-8

Li, W., Teng, X., Chen, X., Liu, L., Xu, L., Zhang, J., Wang, Y., Zhang, Y., Shi, Z., 2021. Organic Coating Reduces Hygroscopic Growth of Phase-Separated Aerosol Particles. Environ. Sci. Technol. 55, 16339–16346. https://doi.org/10.1021/acs.est.1c05901

Lingaswamy, A.P., Nishanth, T., Kumar, T.V.L., Kumar, M.K.S., 2022. Variations in mixing states of organic aerosol composition and formation of secondary organic aerosol at background region. J. Atmos. Chem. https://doi.org/10.1007/s10874-022-09445-0

Liu, P., Song, M., Zhao, T., Gunthe, S.S., Ham, S., He, Y., Qin, Y.M., Gong, Z., Amorim, J.C., Bertram, A.K., Martin, S.T., 2018. Resolving the mechanisms of hygroscopic growth and cloud condensation nuclei activity for organic particulate matter. Nat. Commun. 9, 4076. https://doi.org/10.1038/s41467-018-06622-2

Myhre, G., Shindell, D., Bréon, F.-M., W. Collins, J.F., Huang, J., Koch, D., Lamarque, J.-F., Lee, D.,

Mendoza, B., Nakajima, T., Robock, A., Stephens, G., Takemura, T., Zhang, H., 2013. Climate Change 2013: The Physical Science Basis. Contribution of Working Group I to the Fifth Assessment Report of the Intergovernmental Panel on Climate Change, Chapter 8: Anthropogenic and Natural Radiative Forcing, Climate Change 2013: The Physical Science Basis. Contribution of Working Group I to the Fifth Assessment Report of the Intergovernmental Panel on Climate Change. Cambridge, United Kingdom and New York, NY, USA. https://doi.org/https://doi.org/10.1017/CBO9781107415324.018

Nguyen, Q.T., Kjær, K.H., Kling, K.I., Boesen, T., Bilde, M., 2017. Impact of fatty acid coating on the CCN activity of sea salt particles. Tellus, Ser. B Chem. Phys. Meteorol. 69, 1–15. https://doi.org/10.1080/16000889.2017.1304064

North, G.R., Zhang, F., Pyle, J., 2014. Encyclopedia of Atmospheric Sciences, 2nd ed, Encyclopedia of Atmospheric Sciences: Second Edition. Academic Press, Cambridge, MA.

O'Brien, R.E., Wang, B., Laskin, A., Riemer, N., West, M., Zhang, Q., Sun, Y., Yu, X.-Y., Alpert, P., Knopf, D.A., Gilles, M.K., Moffet, R.C., 2015. Chemical imaging of ambient aerosol particles: Observational constraints on mixing state parameterization. J. Geophys. Res. Atmos. 120, 9591–9605. https://doi.org/10.1002/2015JD023480.Received

Ovadnevaite, J., Zuend, A., Laaksonen, A., Sanchez, K.J., Roberts, G., Ceburnis, D., Decesari, S., Rinaldi, M., Hodas, N., Facchini, M.C., Seinfeld, J.H., O' Dowd, C., 2017. Surface tension prevails over solute effect in organic-influenced cloud droplet activation. Nature 546, 637–641. https://doi.org/10.1038/nature22806

Owen, R.C., Honrath, R.E., 2009. Technical note: a new method for the Lagrangian tracking of pollution

plumes from source to receptor using gridded model output. Atmos. Chem. Phys. 9, 2577–2595. https://doi.org/10.5194/acp-9-2577-2009

Petters, M.D., Carrico, C.M., Kreidenweis, S.M., Prenni, A.J., DeMott, P.J., Collett, J.L., Moosmüller, H., 2009. Cloud condensation nucleation activity of biomass burning aerosol. J. Geophys. Res. 114, D22205. https://doi.org/10.1029/2009JD012353

Petters, M.D., Kreidenweis, S.M., 2013. A single parameter representation of hygroscopic growth and cloud condensation nucleus activity-Part 3: Including surfactant partitioning. Atmos. Chem. Phys. 13, 1081–1091. https://doi.org/10.5194/acp-13-1081-2013

Petters, M.D., Kreidenweis, S.M., 2007. A single parameter representation of hygroscopic growth and cloud condensation nucleus activity. Atmos. Chem. Phys. 7, 1961–1971. https://doi.org/10.5194/acp-7-1961-2007

Petters, S.S., Pagonis, D., Claflin, M.S., Levin, E.J.T., Petters, M.D., Ziemann, P.J., Kreidenweis, S.M., 2017. Hygroscopicity of Organic Compounds as a Function of Carbon Chain Length and Carboxyl, Hydroperoxy, and Carbonyl Functional Groups. J. Phys. Chem. A 121, 5164–5174. https://doi.org/10.1021/acs.jpca.7b04114

Pham, D.Q., O'Brien, R., Fraund, M., Bonanno, D., Laskina, O., Beall, C., Moore, K.A., Forestieri, S., Wang, X., Lee, C., Sultana, C., Grassian, V., Cappa, C.D., Prather, K.A., Moffet, R.C., 2017. Biological Impacts on Carbon Speciation and Morphology of Sea Spray Aerosol. ACS Earth Sp. Chem. 1, 551–561. https://doi.org/10.1021/acsearthspacechem.7b00069

Philip, S., Martin, R. V, Donkelaar, A. Van, Lo, J.W., Wang, Y., Chen, D., Zhang, L., Kasibhatla, P.S., Wang, S., Zhang, Q., Lu, Z., Streets, D.G., Bittman, S., Macdonald, D.J., 2014. Global Chemical Composition

of Ambient Fine Particulate Matter for Exposure Assessment. Environ. Sci. Technol. 48, 13060–13068.

Pöhlker, M.L., Pöhlker, C., Ditas, F., Klimach, T., De Angelis, I.H., Araújo, A., Brito, J., Carbone, S., Cheng, Y., Chi, X., Ditz, R., Gunthe, S.S., Kesselmeier, J., Könemann, T., Lavrič, J. V., Martin, S.T., Mikhailov, E., Moran-Zuloaga, D., Rose, D., Saturno, J., Su, H., Thalman, R., Walter, D., Wang, J., Wolff, S., Barbosa, H.M.J., Artaxo, P., Andreae, M.O., Pöschl, U., 2016. Long-term observations of cloud condensation nuclei in the Amazon rain forest - Part 1: Aerosol size distribution, hygroscopicity, and new model parametrizations for CCN prediction. Atmos. Chem. Phys. 16, 15709–15740. https://doi.org/10.5194/acp-16-15709-2016

Pöschl, U., 2005. Atmospheric aerosols: Composition, transformation, climate and health effects. Angew. Chem. Int. Ed. 44, 7520–7540. https://doi.org/10.1002/anie.200501122

Pringle, K.J., Tost, H., Pozzer, A., Pöschl, U., Lelieveld, J., 2010. Global distribution of the effective aerosol hygroscopicity parameter for CCN activation. Atmos. Chem. Phys. 10, 5241–5255. https://doi.org/10.5194/acp-10-5241-2010

Raveh-Rubin, S., 2017. Dry intrusions: Lagrangian climatology and dynamical impact on the planetary boundary layer. J. Clim. 30, 6661–6682. https://doi.org/10.1175/JCLI-D-16-0782.1

Raveh-Rubin, S., Catto, J.L., 2019. Climatology and dynamics of the link between dry intrusions and cold fronts during winter, Part II: Front-centred perspective. Clim. Dyn. 53, 1893–1909. https://doi.org/10.1007/s00382-019-04793-2

Ren, J., Zhang, F., Wang, Y., Collins, D., Fan, X., Jin, X., Xu, W., Sun, Y., Cribb, M., Li, Z., 2018. Using different assumptions of aerosol mixing state and chemical composition to predict CCN

concentrations based on field measurements in urban Beijing. Atmos. Chem. Phys. 18, 6907–6921. https://doi.org/10.5194/acp-18-6907-2018

Riemer, N., Ault, A.P., West, M., Craig, R.L., Curtis, J.H., 2019. Aerosol Mixing State: Measurements, Modeling, and Impacts. Rev. Geophys. 57, 187–249. https://doi.org/10.1029/2018RG000615

Riemer, N., West, M., 2013. Quantifying aerosol mixing state with entropy and diversity measures. Atmos. Chem. Phys. 13, 11423–11439. https://doi.org/10.5194/acp-13-11423-2013

Roberts, G.C., Day, D.A., Russell, L.M., Dunlea, E.J., Jimenez, J.L., Tomlinson, J.M., Collins, D.R., Shinozuka, Y., Clarke, A.D., 2010. Characterization of particle cloud droplet activity and composition in the free troposphere and the boundary layer during INTEX-B. Atmos. Chem. Phys. 10, 6627–6644. https://doi.org/10.5194/acp-10-6627-2010

Roberts, G.C., Nenes, A., 2005. A continuous-flow streamwise thermal-gradient CCN chamber for atmospheric measurements. Aerosol Sci. Technol. 39, 206–221. https://doi.org/10.1080/027868290913988

Rose, C., Sellegri, K., Moreno, I., Velarde, F., Ramonet, M., Weinhold, K., Krejci, R., Andrade, M., Wiedensohler, A., Ginot, P., Laj, P., 2017. CCN production by new particle formation in the free troposphere. Atmos. Chem. Phys. 17, 1529–1541. https://doi.org/10.5194/acp-17-1529-2017

Rose, D., Gunthe, S.S., Mikhailov, E., Frank, G.P., Dusek, U., Andreae, M.O., Pöschl, U., 2008. Calibration and measurement uncertainties of a continuous-flow cloud condensation nuclei counter (DMT-CCNC): CCN activation of ammonium sulfate and sodium chloride aerosol particles in theory and experiment. Atmos. Chem. Phys. 8, 1153–1179. https://doi.org/10.5194/acp-8-1153-2008

Royer, H.M., Pöhlker, M.L., Krüger, O., Blades, E., Sealy, P., Lata, N.N., Cheng, Z., China, S., Ault, A.P.,

Quinn, P.K., Zuidema, P., Pöhlker, C., Pöschl, U., Andreae, M., Gaston, C.J., 2023. African smoke particles act as cloud condensation nuclei in the wintertime tropical North Atlantic boundary layer over Barbados. Atmos. Chem. Phys. 23, 981–998. https://doi.org/10.5194/acp-23-981-2023

Saleh, R., Marks, M., Heo, J., Adams, P.J., Donahue, N.M., Robinson, A.L., 2015. Contribution of brown carbon and lensing to the direct radiative effect of carbonaceous aerosols from biomass and biofuel burning emissions. J. Geophys. Res. Atmos 120, 10,285–10,296. https://doi.org/10.1002/2015JD023697

Saliba, G., Sanchez, K.J., Russell, L.M., Twohy, C.H., Roberts, G.C., Lewis, S., Dedrick, J., McCluskey, C.S., Moore, K., DeMott, P.J., Toohey, D.W., 2021. Organic composition of three different size ranges of aerosol particles over the Southern Ocean. Aerosol Sci. Technol. 55, 268–288. https://doi.org/10.1080/02786826.2020.1845296

Sánchez Gácita, M., Longo, K.M., Freire, J.L.M., Freitas, S.R., Martin, S.T., 2017. Impact of mixing state and hygroscopicity on CCN activity of biomass burning aerosol in Amazonia. Atmos. Chem. Phys. 17, 2373–2392. https://doi.org/10.5194/acp-17-2373-2017

Schmeissner, T., Krejci, R., Ström, J., Birmili, W., Wiedensohler, A., Hochschild, G., Gross, J., Hoffmann, P., Calderon, S., 2011. Analysis of number size distributions of tropical free tropospheric aerosol particles observed at Pico Espejo (4765 m a.s.l.), Venezuela. Atmos. Chem. Phys. 11, 3319–3332. https://doi.org/10.5194/acp-11-3319-2011

Schulze, B.C., Charan, S.M., Kenseth, C.M., Kong, W., Bates, K.H., Williams, W., Metcalf, A.R., Jonsson, H.H., Woods, R., Sorooshian, A., Flagan, R.C., Seinfeld, J.H., 2020. Characterization of Aerosol Hygroscopicity Over the Northeast Pacific Ocean: Impacts on Prediction of CCN and Stratocumulus

Cloud Droplet Number Concentrations. Earth Sp. Sci. 7, e2020EA001098. https://doi.org/10.1029/2020ea001098

Schum, S.K., Zhang, B., Dzepina, K., Fialho, P., Mazzoleni, C., Mazzoleni, L.R., 2018. Molecular and physical characteristics of aerosol at a remote free troposphere site: Implications for atmospheric aging. Atmos. Chem. Phys. 18, 14017–14036. https://doi.org/10.5194/acp-18-14017-2018

Seibert, P., Frank, A., 2004. Source-receptor matrix calculation with a Lagrangian particle dispersion model in backward mode. Atmos. Chem. Phys. 4, 51–63. https://doi.org/10.5194/acp-4-51-2004

Seinfeld, J.H., Bretherton, C., Carslaw, K.S., Coe, H., DeMott, P.J., Dunlea, E.J., Feingold, G., Ghan, S., Guenther, A.B., Kahn, R., Kraucunas, I., Kreidenweis, S.M., Molina, M.J., Nenes, A., Penner, J.E., Prather, K.A., Ramanathan, V., Ramaswamy, V., Rasch, P.J., Ravishankara, A.R., Rosenfeld, D., Stephens, G., Wood, R., 2016. Improving our fundamental understanding of the role of aerosol-cloud interactions in the climate system. PNAS 113, 5781–5790. https://doi.org/10.1073/pnas.1514043113

Sharma, N., China, S., Bhandari, J., Gorkowski, K., Dubey, M., Zaveri, R.A., Mazzoleni, C., 2018. Physical Properties of Aerosol Internally Mixed With Soot Particles in a Biogenically Dominated Environment in California. Geophys. Res. Lett. 45, 11,473-11,482. https://doi.org/10.1029/2018GL079404

Siebert, H., Szodry, K.-E., Egerer, U., Wehner, B., Henning, S., Chevalier, K., Lückerath, J., Welz, O., Weinhold, K., Lauermann, F., Gottschalk, M., Ehrlich, A., Wendisch, M., Fialho, P., Roberts, G., Allwayin, N., Schum, S., Shaw, R.A., Mazzoleni, C., Mazzoleni, L., Nowak, J.L., Malinowski, S.P., Karpinska, K., Kumala, W., Czyzewska, D., Luke, E.P., Kollias, P., Wood, R., Mellado, J.P., 2021. Observations of Aerosol, Cloud, Turbulence, and Radiation Properties at the Top of the Marine

Boundary Layer over the Eastern North Atlantic Ocean: The ACORES Campaign. BAMS 102, E123–E147. https://doi.org/10.1175/BAMS-D-19-0191.1

Sorooshian, A., Lu, M.L., Brechtel, F.J., Jonsson, H., Feingold, G., Flagan, R.C., Seinfeld, J.H., 2007. On the source of organic acid aerosol layers above clouds. Environ. Sci. Technol. 41, 4647–4654. https://doi.org/10.1021/es0630442

Stevens, R., Dastoor, A., 2019. A review of the representation of aerosol mixing state in atmospheric models. Atmosphere (Basel). 10. https://doi.org/10.3390/atmos10040168

Stier, P., Seinfeld, J.H., Kinne, S., Feichter, J., Boucher, O., 2006. Impact of nonabsorbing anthropogenic aerosols on clear-sky atmospheric absorption. J. Geophys. Res 111, 1–11. https://doi.org/10.1029/2006JD007147

Stohl, A., Forster, C., Frank, A., Seibert, P., Wotawa, G., 2005. Technical note: The Lagrangian particle dispersion model FLEXPART version 6.2. Atmos. Chem. Phys. 5, 2461–2474. https://doi.org/10.5194/acp-5-2461-2005

Su, H., Rose, D., Cheng, Y.F., Gunthe, S.S., Massling, A., Stock, M., Wiedensohler, A., Andreae, M.O., Pöschl, U., 2010. Hygroscopicity distribution concept for measurement data analysis and modeling of aerosol particle mixing state with regard to hygroscopic growth and CCN activation. Atmos. Chem. Phys. 10, 7489–7503. https://doi.org/10.5194/acp-10-7489-2010

Sullivan, R.C., Moore, M.J.K., Petters, M.D., Kreidenweis, S.M., Qafoku, O., Laskin, A., Roberts, G.C., Prather, K.A., 2010. Impact of Particle Generation Method on the Apparent Hygroscopicity of Insoluble Mineral Particles. Aerosol Sci. Technol. 44, 830–846. https://doi.org/10.1080/02786826.2010.497514

Sullivan, R. C., Moore, M.J.K., Petters, M.D., Kreidenweis, S.M., Roberts, G.C., Prather, K.A., 2009. Effect of chemical mixing state on the hygroscopicity and cloud nucleation properties of calcium mineral dust particles. Atmos. Chem. Phys. 9, 3303–3316. https://doi.org/10.5194/acp-9-3303-2009

Sullivan, Ryan C., Moore, M.J.K., Petters, M.D., Kreidenweis, S.M., Roberts, G.C., Prather, K.A., 2009. Timescale for hygroscopic conversion of calcite mineral particles through heterogeneous reaction with nitric acid. Phys. Chem. Chem. Phys. 11, 7826. https://doi.org/10.1039/b904217b

Sun, J., Ariya, P.A., 2006. Atmospheric organic and bio-aerosols as cloud condensation nuclei (CCN): A review. Atmos. Environ. 40, 795–820. https://doi.org/10.1016/j.atmosenv.2005.05.052

Sun, J., Hermann, M., Yuan, Y., Birmili, W., Collaud Coen, M., Weinhold, K., Madueño, L., Poulain, L., Tuch, T., Ries, L., Sohmer, R., Couret, C., Frank, G., Brem, B.T., Gysel-Beer, M., Ma, N., Wiedensohler, A., 2021. Long-term trends of black carbon and particle number concentration in the lower free troposphere in Central Europe. Environ. Sci. Eur. 33. https://doi.org/10.1186/s12302-021-00488-w

Tao, J., Kuang, Y., Luo, B., Liu, L., Xu, H., Ma, N., Liu, P., Xue, B., Zhai, M., Xu, Wanyun, Xu, Weiqi, Sun, Y., 2023. Kinetic Limitations Affect Cloud Condensation Nuclei Activity Measurements Under Low Supersaturation. Geophys. Res. Lett. 50, 1–9. https://doi.org/10.1029/2022GL101603

Tomlin, J.M., Jankowski, K.A., Veghte, D.P., Wang, P., Fraund, M., Weis, J., Zheng, G., Wang, Y., Rivera-adorno, F., Raveh-rubin, S., Knopf, D.A., Wang, J., Gilles, M.K., Moffet, R.C., 2021. Impact of dry intrusion events on the composition and mixing state of particles during the winter Aerosol and Cloud Experiment in the Eastern North Atlantic (ACE-ENA). Atmos. Chem. Phys. 21, 18123–18146.

Unga, F., Choël, M., Derimian, Y., Deboudt, K., Dubovik, O., Goloub, P., 2018. Microscopic Observations

of Core-Shell Particle Structure and Implications for Atmospheric Aerosol Remote Sensing. J. Geophys. Res. Atmos. 123, 13,944-13,962. https://doi.org/10.1029/2018JD028602

Val Martin, M., Honrath, R.E., Owen, R.C., Li, Q.B., 2008. Seasonal variation of nitrogen oxides in the central North Atlantic lower free troposhere. J. Geophys. Res. 113, 1–15. https://doi.org/10.1029/2007JD009688

Vestin, A., Rissler, J., Swietlicki, E., Frank, G.P., Andreae, M.O., 2007. Cloud-nucleating properties of the Amazonian biomass burning aerosol: Cloud condensation nuclei measurements and modeling. J. Geophys. Res. 112, 1–16. https://doi.org/10.1029/2006JD008104

Wang, J., Cubison, M.J., Aiken, A.C., Jimenez, J.L., Collins, D.R., 2010. The importance of aerosol mixing state and size-resolved composition on CCN concentration and the variation of the importance with atmospheric aging of aerosols. Atmos. Chem. Phys. 10, 7267–7283. https://doi.org/10.5194/acp-10-7267-2010

Wang, Yuan, Niu, S., Lv, J., Lu, C., Xu, X., Wang, Yuying, Ding, J., Zhang, H., Wang, T., Kang, B., 2019. A New Method for Distinguishing Unactivated Particles in Cloud Condensation Nuclei Measurements: Implications for Aerosol Indirect Effect Evaluation. Geophys. Res. Lett. 46, 14185–14194. https://doi.org/10.1029/2019GL085379

Wex, H., Dieckmann, K., Roberts, G.C., Conrath, T., Izaguirre, M.A., Hartmann, S., Herenz, P., Schäfer, M., Ditas, F., Schmeissner, T., Henning, S., Wehner, B., Siebert, H., Stratmann, F., 2016. Aerosol arriving on the Caribbean island of Barbados: physical properties and origin. Atmos. Chem. Phys. 16, 14107–14130. https://doi.org/10.5194/acp-16-14107-2016

Wiedensohler, A., Birmili, W., Nowak, A., Sonntag, A., Weinhold, K., Merkel, M., Wehner, B., Tuch, T.,

Pfeifer, S., Fiebig, M., Fjäraa, A.M., Asmi, E., Sellegri, K., Depuy, R., Venzac, H., Villani, P., Laj, P., Aalto, P., Ogren, J.A., Swietlicki, E., Williams, P., Roldin, P., Quincey, P., Hüglin, C., Fierz-Schmidhauser, R., Gysel, M., Weingartner, E., Riccobono, F., Santos, S., Grüning, C., Faloon, K., Beddows, D., Harrison, R., Monahan, C., Jennings, S.G., O'Dowd, C.D., Marinoni, A., Horn, H.G., Keck, L., Jiang, J., Scheckman, J., McMurry, P.H., Deng, Z., Zhao, C.S., Moerman, M., Henzing, B., De Leeuw, G., Löschau, G., Bastian, S., 2012. Mobility particle size spectrometers: Harmonization of technical standards and data structure to facilitate high quality long-term observations of atmospheric particle number size distributions. Atmos. Meas. Tech. 5, 657–685. https://doi.org/10.5194/amt-5-657-2012

Williamson, C.J., Kupc, A., Axisa, D., Bilsback, K.R., Bui, T., Campuzano-jost, P., Dollner, M., Froyd, K.D., Hodshire, A.L., Jimenez, J.L., Kodros, J.K., Luo, G., Murphy, D.M., Nault, B.A., Ray, E.A., Weinzierl, B., Wilson, J.C., Yu, F., Yu, P., Pierce, J.R., Brock, C.A., 2019. A large source of cloud condensation nuclei from new particle formation in the tropics. Nature 574, 399–403. https://doi.org/10.1038/s41586-019-1638-9

Wu, Z.J., Zheng, J., Shang, D.J., Du, Z.F., Wu, Y.S., Zeng, L.M., Wiedensohler, A., Hu, M., 2016. Particle hygroscopicity and its link to chemical composition in the urban atmosphere of Beijing, China, during summertime. Atmos. Chem. Phys. 16, 1123–1138. https://doi.org/10.5194/acp-16-1123-2016

Yu, J.Z., Huang, X.F., Xu, J., Hu, M., 2005. When aerosol sulfate goes up, so does oxalate: Implication for the formation mechanisms of oxalate. Environ. Sci. Technol. 39, 128–133. https://doi.org/10.1021/es049559f

Zhang, B., Owen, R.C., Perlinger, J.A., Helmig, D., Val Martin, M., Kramer, L., Mazzoleni, L.R., Mazzoleni,

C., 2017. Ten-year chemical signatures associated with long-range transport observed in the free troposphere over the central North Atlantic. Elem. Sci. Anth. 5, 194. https://doi.org/10.1525/elementa.194

Zhang, B., Owen, R.C., Perlinger, J.A., Kumar, A., Wu, S., Val Martin, M., Kramer, L., Helmig, D., Honrath, R.E., 2014. A semi-Lagrangian view of ozone production tendency in North American outflow in the summers of 2009 and 2010. Atmos. Chem. Phys. 14, 2267–2287. https://doi.org/10.5194/acp-14-2267-2014

Zhao, D.F., Buchholz, A., Kortner, B., Schlag, P., Rubach, F., Kiendler-Scharr, A., Tillmann, R., Wahner, A., Flores, J.M., Rudich, Y., Watne, A.K., Hallquist, M., Wildt, J., Mentel, T.F., 2015. Size-dependent hygroscopicity parameter (κ) and chemical composition of secondary organic cloud condensation nuclei. Geophys. Res. Lett. 42, 10920–10928. https://doi.org/10.1002/2015GL066497

Zheng, G., Sedlacek, A.J., Aiken, A.C., Feng, Y., Watson, T.B., Raveh-Rubin, S., Uin, J., Lewis, E.R., Wang, J., 2020. Long-range transported North American wildfire aerosols observed in marine boundary layer of eastern North Atlantic. Environ. Int. 139, 105680. https://doi.org/10.1016/j.envint.2020.105680

Zhou, S., Collier, S., Jaffe, D.A., Zhang, Q., 2019. Free Tropospheric Aerosols at the Mt. Bachelor Observatory: More Oxidized and Higher Sulfate Content Compared to Boundary Layer Aerosols. Atmos. Chem. Phys. 19, 1571–1585. https://doi.org/10.5194/acp-2018-821

Zufall, M.J., Davidson, C.I., 1998. Dry Deposition of Particles from the Atmosphere, in: Linkov, I., Wilson, R. (Eds.), Air Pollution in the Ural Mountains: Environmental, Health and Policy Aspects. Springer, Dordrecht, pp. 55–56. https://doi.org/doi.org/10.1007/978-94-011-5208-2_5